SAT

FINAL REPORT

E86-10018

NASA-CR-176425

NASA CONTRACT NAS5-27595

SYSTEMATIC AND RANDOM VARIATIONS IN DIGITAL THEMATIC MAPPER DATA

M.J. Duggin and H. Sakhavat

TABLE OF CONTENTS

INTRODUCTION

Radiance recorded by any remote sensing instrument will contain noise which will consist of both systematic and random variations. Systematic variations may be due to sun-target-sensor geometry (e.g. Duggin 1985a, Kirchner and Schnetzler 1981) atmospheric conditions (e.g. Dave 1978, 1980, Schnetzler 1981) and the interaction of the spectral characteristics of the sensor with those of upwelling radiance (e.g. Slater 1979, Duggin, Slater and Somers 1980, Duggin 1985 a,b, Markham and Barker, 1985). Random variations in the data may be caused by variations in the nature and in the heterogeneity of the ground cover (e.g. Daughtry, Vanderbilt and Pollara 1982, Duggin 1974, 1983, 1985 a,b), by variations in atmospheric transmission, and by the interaction of these variations with the sensing device (e.g. Duggin 1985a).

It is important to be aware of the extent of random and systematic errors in recorded radiance data across ostensibly uniform ground areas in order to assess the impact on quantitative image analysis procedures for both the single date and the multidate cases. It has been shown that random variations in irradiance and in reflectance characteristics (caused, for example, by variations in the nature and in the heterogeneity of ground cover) can cause variations in the discriminability of vegetation stress (Duggin 1983) and that random variations in unresolved (sub-pixel sized) cloud can affect discriminability of agricultural targets (Duggin, Schoch, Cunia and Piwinski 1984). Duggin and Schoch (1984) and Wardley (1984) showed that the impact of random variations in irradiance, ground reflectance and atmospheric transmittance on target discriminability can be angle-dependent. Systematic variations in radiance due to scan angle have been observed by many workers in, for example, even MSS data with a scan angle range of 11.56 (Kaneko and Engvall 1977) and in AVHRR data which has a much larger scan angular range of 55 (e.g.

Duggin and Saunders 1984, Duggin and Piwinski 1984). The cause of the angular dependence of spectral radiance (and therefore of discriminability) is the systematic variation in the reflectance properties of ground cover with illumination and with viewing angles (e.g. Bauer, et al. 1979, Coulson 1966, Coulson et al. 1965, Duggin 1977, Egbert and Ulaby 1972, Kollenkark et al. 1982, Smith 1979, 1983, Suits and Safir 1972). In the case of emitted radiance, there is a dependence of emissivity on view angles (e.g. Jackson 1981, Kimes, et al. 1980, Kimes and Kirchner 1983, Kimes 1981a,b 1983). Atmospheric scattering and transmission also vary with viewing and with illumination angles (e.g. Turner 1978, Dave 1978). The combination of these systematic variations in factors controlling radiance levels gives rise to upwelling radiance which varies with viewing geometry in a target-dependent manner (e.g. Kirchner and Schnetzler 1981, Schnezler 1981, Duggin, 1985, Duggin, Lindsay and Sakhavat 1985, Duggin, Sakhavat and Lindsay 1985). There is the possibility that systematic effects may be corrected for if they are properly understood.

It has been reported that there is a sensor dependent variation of about 2% in radiance levels across the TM scan line in a manner which is scan direction-dependent (Malila, et al 1984, Metzler and Malila 1985, Kieffer, et al 1985, Murphy, et al 1985). This effect will compound the effect of the scan angle dependence of sensor output which is due to the goniometric anisotropy of the scene radiance. The angle-dependent upwelling scene radiance may interact with both the spectral and spatial characteristics of the sensor in an as-yet undetermined manner (e.g. Duggin 1985a,b): we do not yet know whether this is a first order or a higher order effect.

It was our intention in this study to examine the systematic and the random variations in digital radiance data recorded in each band by the thematic mapper over crop areas which were ostensibly uniform and which were free from visible cloud. The thematic mappers on Landsats 4 and 5 have narrower bandpasses and a

wider range of wavebands than the MSS or the AVHRR and so findings for the MSS and for the AVHRR cannot automatically be assumed to apply to the TM, even though the scan angle range for the AVHRR be restricted to that of the TM. For example, the superior spatial resolution of the TM (30 m as compared to 79 m for the MSS and 1 km for the AVHRR) will increase the random variation between radiance values recorded from individual pixels located in apparently uniform areas (e.g. Daughtry, Vanderbilt and Pollara 1982).

The analysis was performed on several scenes at different growth stages. We considered agricultural areas. We wished to see if there were seasonal effects upon both random and systematic variations in digital radiance data recorded in the thematic mapper bandpasses.

The heterogeneity of the scene within the ground resolution cell, which is imaged by the IFOV will affect the sensor output in each bandpass and will affect the spectral distribution of sensor outputs for each pixel. This is because of the spatial distribution of different scene elements with different optical properties and anisotropies within the IFOV. The scene elements will interact with the rear-projected point spread function of the TM system onto the object plane in a manner which is both spatially and spectrally-dependent. This has been discussed by (Duggin 1985a,b) and will be dealt with in greater detail later in this report. The variation in scene type, and in the distribution of scene components across the area imaged by the TM will superimpose random variations in the level and in the spectral (between-band) radiance distribution. Such variations in scene composition across the imaged area will also give rise to edge effects. The impact of the edge effects will depend not only on the nature of the contrasting composition of adjoining ground resolution cells, but will also depend upon the angle through which the imaged area is viewed and upon the interaction of the upwelling radiance with the spectral and spatial characteristics of the TM sensors.

The edge effects will impact the TM radiance data (calibrated digital counts) in a manner which is dependent upon the modulation transfer function (MTF) of the TM in each bandpass for each sensor (e.g. Schowengerdt, Archwametry and Wrigley 1985, Cushnie and Atkinson, 1985). The Fourier transform of the MTF describes the instantaneous rear-projected point spread function (PSF) on the object plane, as will be discussed later.

The radiometric calibration of the TM data has been the focus of several studies (e.g. Tilton, Markham and Alford 1985, Desachy, et al 1985, Schott and Volchok 1985, Murphy, et al 1985, Singh 1985, Duggin 1985b). There has also been considerable effort to develop algorithms to destripe and to radiometrically correct the data after acquisition (e.g. Bernstein, et al 1984, Poros and Peterson 1985, Malaret, et al 1985, Wrigley, et al 1984, 1985). Some considerations will be discussed here.

There have been studies to evaluate the multivariate statistical analysis of digital TM multiband, multitemporal data for improved land use analysis (e.g. Anuta, et al 1984, Forster, et al 1985). Studies of the analysis of eigenvectors of the principal components of multitemporal, multichannel TM data will be discussed in an appendix as a potential means for enhanced land use discrimination.

ANALYSIS

In this analysis, we were constrained by data availability; the data which we hoped to obtain at various stages over agricultural regions including one in Iowa (path=27, row=31 on the World Reference System (WRS)) was not available at all of the growth stages requested. Some acquisitions were cloudy and unforeseen circumstances prevented the acquisition of other scenes in time to perform the analysis for this report. We did analyze two images over a forested area, however.

The images which we discuss in this report are restricted to three regions. In each case, we used radiometrically corrected p-type CCT data (NASA 1983). WRS path 27, row 31 covers a corn/soybean region in Iowa: in August 1982, only 4 band data was available for this area.

Firstly, in each case, the data were screened using the Landsat Assessment System for cloud and for uniformity. That is, to ensure that the scene did indeed consist entirely of crop areas for those regions examined. Only the roads between fields were not vegetated for the agricultural areas studied.

In the first analysis, a mask was generated. Three swaths were used across the full image: each was 300 lines deep and started at lines 500, 1900 and 5000. Slices which were 16 pixels wide were taken in these swaths. The slices had starting pixel numbers 300 (bottom two swaths) 500, 1000, 2000, 3000, 4000, 5000, 6000, 6500, 6700 (top two swaths). The offset is related to the Earth rotation correction of the Landsat image. In this manner, a non-biased analysis was performed by analyzing all of the pixels in each slice over an apparently uniform, cloud-free agricultural region. Training within these regions on areas which appeared uniform on the image was not performed in this analysis, as it was considered that this would have resulted in bias deriving from unsubstantiated, a priori assumptions as to the nature of the target. The mean

digital counts for each slice were calculated for each bandpass. The digital counts were used since we were interested in variations within images and considered that errors due to offset would not seriously affect our estimates of coefficients of variation (standard deviation divided by the mean; C.V.) in radiance, except to alter the C.V. by about 15% in the case of TM band 6 (Barker 1984, Barker et al 1984). At the same time, the variance and the coefficient of variation were calculated for each slice. Fig. 1 shows the mean digital radiance values for the first four bandpasses of the August 02 image for path 27, row 31. Only four bands were available for analysis for this image. The mean radiance values are shown as a function of scan angle (starting pixel value for the slice) and of mean scan line for the swath from which the slices were taken. In this and in all subsequent figures, the northernmost swath (lower mean line number) is closest to the viewer, west is to the left (lowest pixel number) and east is to the right (highest pixel number). There was no attempt to register images in this investigation.

It is seen that there is a significant systematic variation with scan angle before harvest, with a superimposed random variation of about 5%. The systematic variation is over 10% between the edges and the center of the image and is apparently close to symmetric about nadir for TM band 1 of the pre-harvest image. The effect becomes more pronounced in band 2 and is almost 25% in band 3. There is a strongly assymmetric 30% change across the image for TM band 4 of the same image. There appears to be a general decrease in mean pixel radiance from south (mean scan line 5150) to north (mean scan line 650) in this image, coupled with some change in the apparent scan angle dependence. Also shown are the coefficients of variation (C.V.s) for the pixel radiance values contained within each slice of each single-band image. The C.V.s are also plotted as a function of pixel and mean scan line for the slices considered in the mask superimposed on the image. There is approximately a 50% variation in

C.V. about nadir for bands 1 through 3, with a superimposed random variation in the C.V. and a systematic decreasing trend towards the north portion of the image (decreasing mean scan line). Band 4 (the reflected infrared region) shows mainly random variation with a slight monatonically increasing trend in C.V. from west to east. It is noteworthy that the C.V. is generally less than 10% for band 1 and 15% for band 2 but rises to nearly 30% for band 3 (whose digital values are lower than bands 1 or 2), falling back to less than approximately 17% in band 4. There does appear to be a general trend for the C.V. to decrease from south to north.

The same region (path 27, row 31) was viewed again after harvest (October 21, 1982). A color infrared rendition of this image on the interactive computer screen suggested that this area was mostly stubble. The mean digital counts for the seven band data are shown in Fig. 2 as a function of the same variables as for Fig. 1. They appear to show a general trend decreasing approximately 10% from west to east in the image. The reverse is the case in band 6, the thermal infrared channel. There appears to be a slight decreasing trend in radiance values from south to north in the image and the noise (random variation) in digital radiance values appears to be approximately 10%. The digital values are lower after harvest, except in band 3. The coefficients of variation for this image are shown as a function of pixel and mean scan line in Fig. 3. They are all slightly higher than in the case of the pre-harvest image for the first four bands, are around 20% in band 5, 20% in band 7, but less than 5% in band 6. However, there is an apparently anomalous increase in C.V. at the far east side of the image, which was not readily explicable from image data of the slices examined on the interactive computer screen. The most obvious possibility would be a greater heterogeneity in ground cover at the eastern edge of the scene. For this image, an examination of the scene and of the analyzed slices in a

false color rendition on the interactive computer screen suggested that patches of vigorous vegetation existed in what appeared to be stubble or soil areas. The distribution of these scene elements might have, for some reason, been more heterogeneous towards the extreme east of the image.

The same area (path 27, row 31) was examined using a later (Landsat 5) acquisition obtained on August 15, 1984 (image number 5016716293). For this image, in order to avoid slight, localized cumulus cloud it was necessary to start the three swaths at lines 2072, 3900 and 4900. Mean digital radiance values are shown for the test areas (slices) as a function of pixel and of mean scan line in Fig. 4. Bands 1-4 show weaker systematic trends than the August 02, 1982 image of the same area. Random variation appears generally to be of the order 5% in digital radiance values, while there is no obvious symmetry in the systematic component of variations in bands 1-3. Band 4 shows approximately a 20% decrease in radiance for the southern portion of the image, but no such trend in the middle or for the northern region. The dependence on mean scan line seems pronounced only for bands 5-7. Band 6 does show the same general increase to the east as for the October 1982 image, analyzed in Fig. 2.

Fig. 5 shows the coefficients of variation of the pixel radiance values for the windowed areas (slices) described by the overlay mask, plotted as a function of pixel and of mean line. The C.V.s are below 0.08 for band 1 and generally below 0.10 for band 2, with a random variation of up to 30% and with only a slight systematic decreasing trend to the northeast. In band 3, the C.V. is 0.25 at the west edge of the image, falling to 0.15 or less towards the east. The decrease is more pronounced in the north of the image than is the case in the south. In band 4, the C.V. is generally less than 0.18, with a random variation of up to 20% and a slight decrease from west to east in the south of the image. The situation is similar in band 5. The thermal infrared band, TM6, shows C.V. values less than 0.04, which exhibit a general decrease in trend from

west to east in the south of the image, and a general decrease from south to north, which is more pronounced in the east of the image. Band 7 has higher C.V. values (up to 0.40). There is a decrease from west to east and a slight decreasing trend from south to north. However, while the thermal IR band (6) shows the northeast region of the image to exhibit the lowest variance, bands 4, 5 and 7 (reflected-to mid-IR) show high variance. This may indicate a higher heterogeneity in growth stage in this region.

The analysis on the August 1982 image, when compared to that performed on the August 1984 image suggests that the systematic variations across an image depend upon time. This may be related to the substantial non-uniform changes with Julian date in both the level and angular dependence of radiance recorded over the crop areas of the U.S. Great Plains by the AVHRR, as reported by (e.g.) Duggin and Piwinski (1984). Atmospheric changes and variations at ground level can occur between image acquisitions.

Factors contributing to radiance changes across an image are atmospheric changes across the imaged area, together with atmospheric scattering anisotropy and hemispherical-conical spectral reflectance anisotropy which is dependent on sun-target-sensor geometry, as mentioned earlier. However, while these effects will be substantial for a large scan angle range, covering a large area, such as the AVHRR ($\pm 55^{0}$), one would expect these effects to be less for the TM, whose scan angle range is only $\pm 7.7^{0}$.

It has been noted (Duggin 1974, 1983) that the random variation to be expected in recorded radiance will arise partly from random variations in atmospheric transmission and partly from variations in irradiance: reported coefficients of variation are approximately 6% (Duggin 1974, 1983). It has also been reported (Duggin 1983) that ground reflectance measurements made at 80 m spacings in the MSS bandpasses show between 5% and 20% coefficient of variation.

Systematic recorded radiance due to atmospheric scattering and bidirectional reflectance factors anisotropy might be expected to give rise to substantial scan angle dependence for large scan angle ranges (such as $\pm 55^0$ for the AVHRR). However, random variations might be expected to predominate over systematic variations for the smaller scan angular range ($\pm 7.7^0$) for the thematic mapper. It is also interesting to note that the range of random variation before and after harvest in 1982 is not markedly different and that the same range of variation appears to apply to the August 1984 images.

We now tried a different technique, involving "training" within the grid cell areas described above. The same mask (overlay) was employed as in the method described above in order to define slices 16 pixels wide by 300 lines deep. However, in this analysis, we used the cursor whose size, shape and position could be defined interactively to "train" on areas considered to consist of the most vigorous vegetation because of their red hue and saturation when the interactive display was used with appropriate look up tables (LUT's) in the following modes:

(i) TM 2 = blue
TM 3 = green — best for agricultural scene
TM 4 = red

(ii) TM 4 = red
TM 5 = green — best for forest scene - separates forest from grassland and agricultural areas
TM 7 = blue

Each "slice" on each "swath" was taken to be a class, and training was performed on three vigorous vegetation sites in each class, or slice. In this analysis, we did make the assumption that what appeared to be "red" on the monitor was vigorous vegetation, so that this was a biased analysis.

The cursor mode was used on the LAS interactive analysis terminal (IAT) in order to enclose those areas identified (a priori) by means of their appearance

in a false color mode. The central point of the examined area was obtained (both screen coordinates and coordinates related to the master image) from the IAT control monitor, using the POLYSIT2 program. While the number of pixels enclosed in each slice was always constant, this quantity varied in the case of individually located and positioned cursors.

The analysis described above was used on the pre-harvest Fort Dodge images (path 27, row 31, image # 4001716261, 02 August 1982). Three training sites on apparently vigorous vegetation were selected in each slice and the data for the pooled sites in each slice are presented here. Fig. 6 shows the variation with pixel number (scan angle) of the mean digital radiance values for each training site, in each bandpass. Swath X has a line start (first line of swath) of 500, swath Y of 2000 and swath Z of 5000. Mean pixel radiance values for each of the two training areas within each grid cell, as well as the mean of the means of the two training areas or cells (for which the best fit curve is shown) are displayed. The scan angle-dependence is larger than in the case for the previous analysis. Scan angle effects of up to 20% are seen in TM bands 1 to 3, but the effects in TM band 4 are anisotropic about nadir, and exceed 20%. The reason for the difference in the results of the two analyses is probably due to the fact that the method involving no training on apparently vegetated areas includes areas which are less vegetated, or areas whose leaf area index is less than that in areas (subjectively) selected in this (interactive) analysis. When training is employed, an assumption is made that vegetation vigor is related to hue and to saturation perceived on the screen of the image analysis terminal. Training within the (18 x 300 pixel) grid cell areas was also used for the seven band post-harvest data for the same scene (path 27, row 31 image # 4009716273, 21 October 1982). The data for the X swath (line start 500) is shown only in Fig. 7. It is seen that there is far less variation than was the case before harvest. This is to be expected, since the scene consists mainly of stubble.

An examination of a post harvest Indianapolis, Indiana scene (image # 4010315505, 27 November, 1982) showed similar results to the post harvest Webster-Fort Dodge image (path 27, row 31 image # 4009716273). The plot of the mean digital counts for each of the grid cells as a function of start pixel is shown in Fig. 8, and exhibits the same general behavior as shown for image # 4009716273, the post-harvest image for path 27, row 31. The plot of the coefficients of variation in digital counts for each bandpass, for each 16 pixel by 300 line grid cell, displayed as a function of start pixel, is shown in Fig. 9.

We examined an image of forest at Jamestown. We did not train within the grid cells. The image number was 4004315244, August 28, 1982. One swath was taken across the image at (approximately) line 5000. The swath was chosen so that the slices contained forest and minimal cloud. When the "slices" (16 x 300 pixels each) were displayed in composite form on the IAT, a very strong angle-dependence was obvious to the eye. The coefficient of variation for the mean digital count in each band and for each slice was generally less than 15%. Fig. 10 shows the large anisotropic scan angle-dependence of the mean digital counts: the effect is approximately 30% in the case of TM band 3. TM band 4 shows scatter. Fig. 11 shows the coefficient of variation (C.V.) for the digital radiance values, plotted as a function of scan angles. The scan angle-dependence of the C.V. is approximately a factor of two for several bands. The procedure of training on areas of apparently high vegetation was tried for the same area, imaged September 13, 1982 (path 17, row 31, image # 4005915251). Significant, but somewhat less scan angle dependence was found in this case, as is shown in Fig. 12 for the mean values. TM 4 again showed scatter, while TM 6 showed anisotropic behavior. The points for the individual training areas were closer to the best-fit line for the pooled data than was the case for the post-harvest agricultural data. The scan angle-dependence of the coefficient of variation is shown in Fig. 13.

COMMENTS ON THE INTERCALIBRATION OF MULTISENSOR, MULTITEMPORAL, MULTICHANNEL DIGITAL RADIANCE DATA

In order to compare recorded radiance data obtained on the same date using different sensors, or on different dates using either the same sensor or a combination of sensors such as the Landsat 4 and 5 sensors TM 4 and TM 5, it is necessary to refer such data to a common datum. This point is discussed in Duggin 1985b.

While calibration is readily made for a sensor in which the gain and offset have been adjusted during operation (e.g. U.S. Geological Survey 1979, 1984, Duggin 1981), the intercomparison between sensors with different spectral responses (bandpasses) is more complex (e.g. Duggin 1980, 1981, 1985; Slater 1979). This is because of the interaction of the spectral response of the sensor with the spectral radiance incident upon the sensor and because different sensors may record information in different parts of the spectrum, where the upwelling radiance has different values. This point is shown for a hypothetetical situation in Fig 14. Here bandpasses A and B from instrument 1 are taken to be approximately equal to bandpass C of instrument 2. The bandpass of a sensor is normally taken to be the wavelength region between the boundaries where the sensor has a 50% response. It is seen that the spectral regions between the half-power wavelength limits of bandpass A of instrument 1(λ_{1A} , λ_{2A}) and between the half-power wavelength limits of bandpass B of instrument 1(λ_{1B} , λ_{2B}) are not (in sum) the same as that encompassed by the half-power wavelength limits of bandpass C of instrument 2(λ_{1C} , λ_{2C}). The spectral band shapes of the sensor response curves also differ and so the calibrated, summed outputs of the two bandpasses (A and B) of instrument 1 are

$$V_1 = \frac{1}{b_A}\left[\frac{\int_{\lambda_{A0}}^{\lambda_{A'0}} I_A(\lambda)\cdot L(\lambda)\cdot d\lambda}{\int_{\lambda_{A0}}^{\lambda_{A'0}} I_A(\lambda)\cdot d\lambda} - a_A\right] + \frac{1}{b_B}\left[\frac{\int_{\lambda_{B0}}^{\lambda_{B'0}} I_B(\lambda)\cdot L(\lambda)\cdot d\lambda}{\int_{\lambda_{B0}}^{\lambda_{B'0}} I_B(\lambda)\cdot d\lambda} - a_B\right]. \quad (1)$$

while the calibrated output of instrument 2 is

$$V_2 = \frac{1}{b_C}\left[\frac{\int_{\lambda_{C0}}^{\lambda_{C'0}} I_C(\lambda)\cdot L(\lambda)\cdot d\lambda}{\int_{\lambda_{C0}}^{\lambda_{C'0}} I_C(\lambda)\cdot d\lambda} - a_C\right]. \quad (2)$$

Here a_A, a_B and a_C are the offsets of the sensors in bandpasses A, B and C for the two instruments. Also, $1/b_A$, $1/b_B$ and $1/b_C$ are the gains of the sensors with bandpasses A, B and C. $\lambda_{A'0}$, $\lambda_{B'0}$ and $\lambda_{C'0}$ are the upper zero power wavelengths for the sensors, while λ_{A0}, λ_{B0} and λ_{C0} are the lower zero power wavelengths, respectively.

If $L(\lambda)$ changes, which could be as a result of different viewing and illumination geometry (e.g. Kollenkark, et al 1982, Duggin 1985a, Smith 1983) then the interaction between $L(\lambda)$ and $I(\lambda)$ will vary in an instrument-dependent manner. Thus, intercalibrations between the outputs from bands A and B of instrument 1 and band C of instrument 2 depend upon the spectral scene radiance and may therefore change with view angle across even a homogeneous scene. The intercalibrations will also be affected by unresolved cloud, which will modify $L(\lambda)$. However, such intercomparisons are wavelength-specific. The calibrated outputs from channels A and B of instrument 1 will vary differently from each other and from that of channel C of instrument 2. Therefore, the intercomparison must be target-dependent, view angle-dependent and atmosphere-dependent, as well as illumination angle dependent (in the optical-reflective region). The same principles of the above argument would apply if radiance data from two

basically similar sensors (each possessing one similar band pass) on two different instruments were being compared.

Further, as pointed out by Forshaw, et al (1983), by Duggin (1985a) and by Duggin and Schoch (1983), the output of a given sensor depends not only upon the nature of the target and its heterogeneity, but upon the relative location of scene elements of different optical properties and anisotropies in the nominal instantaneous field of view (IFOV) of the sensor. This is because of the interaction of the point-spread function (PSF) of the sensor with the radiance recorded from each of the different scene elements in the IFOV. This situation is shown diagrammatically in Fig 15. The scene is considered to consist of three components A, B and C which give rise to different radiance levels at the sensor (bandpass r) whose point-spread function is shown. The PSF fall-off to zero is generally Gaussian and so radiance may be recorded from very bright scene elements beyond the nominal IFOV of the sensor. The sensor output for a pixel will therefore depend upon the position of the PSF peak with respect to the assemblage of scene elements.

As pointed out by Duggin and Schoch (1983) for a cloud-free image consisting of n different reflecting elements, each occupying a fractional area a_η of a pixel (IFOV), the recorded radiance in bandpass r is, for the optical-reflective region, given by

$$L_r(\theta',\phi') = \frac{\int_{\lambda_{a0}}^{\lambda_{a\omega}} I(\lambda)\left(\int_0^{\tau}\int_{-\pi/2}^{\pi/2}\left\{E(\theta,\phi,\lambda)\int_0^X\int_0^Y [g_1(x,y)\,R_1(\theta,\phi;\theta',\phi',\lambda)P_1(x,y) + g_2(x,y)\,R_2(\theta,\phi;\theta',\phi',\lambda)P_2(x,y) + \ldots + g_n(x,y)\,R_n(\theta,\phi,\theta',\phi',\lambda)P_n(x,y)]\,\tau(\theta',\phi',\lambda)dydx\right\}d\theta d\phi + L_p(\theta_1,\phi_1;\theta_1',\phi_1',\lambda)\right)d\lambda}{\int_{\lambda_{a0}}^{\lambda_{a\omega}} I(\lambda)\cdot d\lambda}, \quad (3)$$

where $I(\lambda)$ is the spectral response of the sensor and $\lambda_{A0}, \lambda_{A0}$, are the lower and upper zero power bandpass limits of the sensor (e.g., bandpass A), respectively

$E(\theta, \phi, \lambda)$ is the scalar global spectral radiance incident on the pixel

$\tau(\theta', \phi', \lambda)$ is the atmospheric transmission along the path from the pixel to the sensor

$R_n(\theta, \phi ; \theta', \phi', \lambda)$ is the spectral hemispherical-conical reflectance factor for scene element n, which occupies fractional area a_n of the heterogeneous pixel

$P_r(x,y)$ is the point-spread function at position x,y in the pixel

$g_n(x,y)$ is a delta function which equals 1 if scene element n is present at (s,y), but is otherwise zero, so that for an IFOV of dimensions X,Y.

$$\int_0^X \int_0^Y g_n(x,y)dydx = a_n;$$

$L_p(\theta_1, \phi_2 ; \theta'_2, \phi'_1, \lambda)$ is the path radiance for the sun-scattering center-sensor geometry defined by $(\theta_1, \phi_1 ; \theta'_1, \phi'_1)$ which will differ from the sun-target-sensor geometry $(\theta, \phi; \theta', \phi')$.

Clearly, the effect of scene element heterogeneity and disposition (with respect to PSF peak value for a given IFOV) on pixel radiance values and on between-band radiance distribution depends on illumination and on viewing geometry. For multitemporal analysis, this consideration is important in determining the acceptable (fractional pixel) superposition accuracy of multi-date images, so that the above effect does not adversely affect the accuracy of classification procedures.

In the case of unresolved (sub-pixel sized) cloud, equation (4) will be modified by the addition of a term

$$L_v(\theta',\phi') = \frac{\int_{\lambda_{min}}^{\lambda_{max}} I(\lambda)\left[\int_0^{\pi}\int_{-\pi/2}^{\pi/2}\left\{E(\theta,\phi,\lambda)\int_0^{x}\int_0^{y}\left[g_1(x,y)R_1(\theta,\phi;\theta',\phi',\lambda)\,P_1(x,y) + g_2(x,y)\,R_2(\theta,\phi;\theta',\phi',\lambda)\,P_2(x,y) + \ldots\right.\right.\right.}{\left.\left.\left. + g_n(x,y)\,R_n(\theta,\phi;\theta',\phi',\lambda)\,P_n(x,y) + \ldots L_v(\theta',\phi') = + g_c(x,y)\,R_c(\lambda)P_c(x,y)\right]\tau(\theta',\phi',\lambda)dydx\right\}d\theta d\phi + L_p(\theta_1,\phi_1;\theta_1',\phi_1',\lambda)\right]d\lambda}{\int_{\lambda_1}^{\lambda_2} I(\lambda)\cdot dx} \quad (4)$$

where g_C describes the presence or absence of cloud at a location in the pixel and where $R_C(\lambda)$ is the (nearly Lambertian) reflectance factor of cloud.

Similar equations can be developed for the thermal infrared region of the spectrum, where scene radiance is determined by scene element spectral emissivity $\varepsilon(\theta'.\phi'.\lambda)$ instead of by the product of global spectral irradiance $E(\theta, \phi; \theta')$ and the hemispherical-conical spectral reflectance factor $R(\theta.\phi; \theta'.\phi'.\lambda)$.

In summary, more calibration data is required for remote sensing instruments. This should consist of gain, offset, spectral response and point-spread function for each bandpass. This data should be available even where radiance data have been radiometrically corrected, so that it is possible to understand what has been done to the raw radiance data. This information will permit theoretical studies which will lead to the development of sensor intercalibration procedures and to an understanding of the limitations inherent in such intercalibrations. Such studies will improve understanding of the effects of unresolved cloud, viewing and illumination geometry, scene composition and heterogeneity. Perhaps correction procedures for systematic effects (e.g. scan angle differences) may be developed. Procedures for the determination of minimum acceptable image superposition accuracy for the multi-date analysis of

images with various sensor-scene combinations, with assemblages of scene elements with different optical properties and different heterogeneities will also need to be developed.

CONCLUSIONS

This study cannot be considered exhaustive: indeed it is still in progress as the multidate data continues to arrive. However, several conclusions are suggested by this work. While some systematic trends in radiance values with scan angle were observed prior to harvest over a crop area in 1982, the same pattern was not repeated two years later. It appeared that the random variation in mean digital values recorded from 4800 pixel sample areas at regular intervals across an image in three swaths generally exceeded the systematic variations for the three images studied, and that the coefficients of variation were within those which might be expected to occur from prior measurements. The coefficients of variation of the digital values from the 4800 pixel areas selected as regular intervals across an image showed some scan angle dependence, but were more dependent upon bandpass than upon season or upon scan angle. The systematic effects did appear to be significant for a forest area.

Random variations may affect image classification accuracy. Further, uncorrected systematic variations across and between images may impose restrictions on the level of classification accuracy which may reasonably be expected from automated classification of single date or multidate, multichannel digital thematic mapper data for the quantification and identification of terrestrial features in a non-photointerpretive fashion. It is therefore important to understand the restrictions which such variations inherent in the digital radiance data may place upon analyses. To this end, further work is needed in which further empirical studies of digital radiance data are used to determine optimum regimes of data acquisition and analyses for selected feature identification and quantification.

Training on areas of vegetation, selected on the basis of their false-color rendition has been shown to produce indications of random and systematic

variations in digital radiance data for each band pass, within and between images. However, this method is less reliable than a stratified sampling technique, since the method of training biases the data, due to assumed relationships between the image characteristics and ground cover, which may or may not be valid.

The effects of intercalibration between the TM sensors on Landsat 4 and Landsat 5 have been discussed. These are problems which have attracted the attention of other workers as well (e.g. Murphy, et al 1985, Singh 1985, Malaret, et al 1985, Slater 1979, Markham and Barker, 1985). However, there is a need to be aware of the interaction of the spectral response characteristics of the sensor and the spectral characteristics of the upwelling scene radiance (e.g. Duggin 1985a,b), which can give rise to (e.g.) target-dependent, sun angle-dependent striping. There is also a need to reduce data to a common datum level for meaningful intercomparison (as also remarked by Metzler and Malila 1985).

The use of principal components analysis for multitemporal TM data analysis is considered in an investigation performed partly under the auspices of this contract and described in the paper attached in appendix A. There is promise that the evaluation of eigenvectors for certain ground features may enhance discriminability.

Other papers arising from this work are included in appendix B.

ACKNOWLEDGEMENT

In most projects, much depends upon the cooperation of others. This has certainly been the case in this investigation.

We should like to express our appreciation for the cheerful help always provided by the Landsat Science Office and by the staff of the NASA Landsat Assessment System at Goddard Space Flight Center. We especially wish to thank Mark Emmons for help in analysis, Brian Markham for frequent discussion and help and Vincent Salomonson for his continued support. It has always been a pleasure to interact with Harold Oseroff, Locke Stewart and Penny Masuoka. We appreciated the always pleasant and productive collaboration with John Lindsay. We are grateful for the help of all of the above colleagues. This work was supported by NASA contract NAS5-27595. We would like to thank Joyce Carpenter for typing this manuscript.

FIGURE CAPTIONS

Fig. 1. The means and coefficients of variation of digital radiance data for rectangular 4800 pixel sample areas (slices) described in the text, plotted as a function of scan angle (pixel) and of mean scan line for the pre-harvest image #4001716261, path 27, row 31, 02 August 1982. Only four bands of data were available.

Fig. 2 The mean digital radiance values for the rectangular 4800 pixel sample slices of the mask described in the text, plotted as a function of scan angle (pixel) and of mean scan line for the post-harvest image #4009716273, path 27, row 31, October 21, 1982.

Fig. 3. The coefficients of variation of digital radiance data for the rectangular slices plotted as a function of scan angle and of mean scan line for the image shown in Fig. 2.

Fig. 4. The mean digital radiance values for the rectangular sample slices of the mask described in the text, plotted as a function of scan angle (pixel) and of mean scan line for the pre-harvest, August 15, 1984 Landsat 5 thematic mapper image #5016716293, path 27, row 31.

Fig. 5. The coefficients of variation of digital radiance data for rectangular slices defined by the mask plotted as a function of scan angle and of mean scan line for the image shown in Fig. 4.

Fig. 6. The mean digital radiance values for training areas selected within rectangular image sample areas, defined by the mask described in the text. Here the image is that obtained by Landsat 4 on August 02, 1982 for path 27, row 31. "Red 1" and "red 2" refer to mean digital radiance values for individual training areas and "red" refers to the average of the mean values for those training areas within each image 'slice'. 'X' 'Y' and 'Z' refer to 300 line swaths taken across the

north, center and south of the image. The mean digital radiance values for the first four TM bands are plotted as a function of pixel for each swath.

Fig. 7. The mean digital radiance values for apparently vegetated training areas ("red 1" and "red 2") and for averages of the means from those training areas ("red") taken from within rectangular image sample areas defined by the mask described in the text. The heterogeneity within each slice is considerable as the image was obtained October 21, 1982 over a crop area path 27, row 31, where much of the scene consisted of stubble. See Fig. 2 for comparison.

Fig. 8. The mean digital radiance values for the rectangular slices of the mask described in the text, plotted as a function of pixel and mean scan line for the post-harvest November 27, 1982 Landsat 4 image #4010315505, path 21, row 32.

Fig. 9. The coefficients of variation of digital radiance data for 4800 pixel rectangular sample slices defined by the mask described in the text, plotted as a function of pixel and of mean scan line for the image shown in Fig. 8.

Fig. 10. The mean digital radiance values for the rectangular 4800 pixel slices of the 300 line swath starting at line 500 described in the text, plotted as a function of pixel and mean scan line for the August 28, 1982 image of the Jamestown forest area (image #4004315244, path 17, row 31 on the WRS system).

Fig. 11. As Fig. 10, but for the 300 line swath starting at line 2000.

Fig. 12. The mean digital radiance values for apparently vegetated training areas ("red 1" and "red 2"), taken from within rectangular image slices. These were taken across one swath (west to east) of an image, and plotted as a function of pixel. The image (#4005915251) was

obtained by Landsat 4 September 13, 1982 over a forested area, path 17, row 31.

Fig. 13. Coefficients of variation of digital radiance values in each bandpass for the image areas described in Fig. 12.

Fig. 14. Spectral responses of two different remote sensing devices, one of which has two adjacent channels similar in combined wavelength coverage to a single channel on the other device, shown with the upwelling spectral scene radiance.

Fig. 15. Interaction of the rear-projected point spread function of a sensor with a heterogeneous scene composed of elements whose optical properties (and therefore, scene radiance values) differ.

REFERENCES

Anuta, P.E., Bartolucci, L.A., Dean, M.E., Lozano, D.F., Malaret, E., McGillem, C.D., Valdes, J.A. and Valenzuela, C.R., 1984, Landsat-4 MSS and thematic mapper data quality and information content analysis, IEEE Trans on Geoscience and Remote Sensing, GE-22, 222.

Barker, J.L., Ball, D.L., Lenny, K.C. and Walker, J.A., 1984, Pre-launch absolute radiometric calibration of Landsat 4 protoflight thematic mapper, NASA Conference Publication 2326, Vol. 1, pp. 130-139.

Barker, J.L., 1984, Relative radiometric calibration of Landsat TM reflective bands, NASA Conference Publication 2326, Vol. 1, pp. 140-180.

Bauer, M.E., Biehl, L.L., Daughtry, C.S.T., Robinson, B.F., and Stoner, E.R., 1979, AgRISTARS Supporting Research, Final Report NAS9-15466, Vol. 1.

Bernstein, R., Lotspiech, J.B., Myers, H.J., Kolsky, H.G. and Lees, R.D., 1984, Analysis and processing of Landsat-4 sensor data using advanced image processing techniques and technologies, IEEE Trans on Geoscience and Remote Sensing, GE-22, 192.

Coulson, K.L., 1966, Effects of reflection properties of natural surfaces in aerial reconnaissance. Appl. Optics, 5, 905.

Coulson, K.L., Bouricius, C.M., and Gray, E.L., 1965. Optical reflection properties of natural surfaces. J. Geophys. Res., 70, 4601.

Cushnie, J.L. and Atkinson, P., 1985, Effect of spatial filtering on scene noise and boundary detail in thematic mapper imagery, Photogramm. Engrg. and Remote Sensing, 51, 1483.

Daughtry, C.S.T., Vanderbilt, V.C. and Pollara, V.J., 1982, Variability of reflectance measurements with sensor altitude and canopy type. Agronomy Jol., 74, 744.

Dave, J.V., 1978, Extensive data sets of the diffuse radiation in realistic atmospheric models with aerosols and common absorbing gases. Solar Energy, 21, 361.

Dave, J.V., 1980, Effect of atmospheric conditions on remote sensing of a surface nonhomogeneity, Photogrammetric Eng. and Remote Sensing 46, 1173.

Desachy, J., Begni, G., Boissin, B., and Perbos, J., 1985, Investigation of Landsat 4 thematic mapper line-to-line and band-to-band registration and relative detector calibration. Photogramm. Engrg. and Remote Sensing, 51, 1291.

Duggin, M.J., 1974. On the natural limitations of target differentiation by means of spectral discrimination techniques, Proceedings of the Ninth International Symposium on Remote Sensing of the Environment, Ann Arbor, Michigan, pp. 499-516.

Duggin, M.J., 1977, Likely effects of solar elevation on the quantification of changes in vegetation with maturity using sequential Landsat imagery. Appl. Optics, 16, 521.

Duggin, M.J., 1980, Effect of instrument spectral response on use of the Landsat MSS for vegetative disease assessment, Applied Optics, 19, 2081.

Duggin, M.J., 1981, Intercalibration of Landsat 1-3 and NOAA 6 and 7 scanner data, Applied Optics, 20, 3815.

Duggin, M.J. and Schoch, L.B., 1983, The effect of point-spread function interaction with radiance from heterogeneous scenes on multitemporal signature analysis, Landsat-4 Science Investigations Summary, Vol. 2, pp. 64-68.

Duggin, M.J., 1983, The effect of irradiation and reflectance variability on vegetation condition assessment, Int. J. Remote Sensing, 4, 601.

Duggin, M.J. and Piwinski, D., 1984, Recorded radiance indices for vegetation monitoring using NOAA AVHRR data; atmospheric and other effects in multitemporal data sets, Applied Optics 23, 2620-2623.

Duggin, M.J. and Saunders, R.W., 1984, in "Satellite sensing of a cloudy atmosphere", ed. A. Henderson-Sellers, Taylor and Frances, London, pp. 241-284.

Duggin, M.J. and Schoch, L.B., 1984, The dependence of target discriminability on systematic and random variations in recorded radiance. Int. J. Remote Sensing, 5, 505-510.

Duggin, M.J., Schoch, L.B., Cunia, T., and Piwinski, D.J., 1984. The effects of random and systematic variations in unresolved cloud on recorded radiance and on target discriminability. Appl. Optics, 23, 387.

Duggin, M.J., Slater, P.N., and Somers, S.L., 1980, A method for calibrating multispectral scanners to allow for the spectral dependence of instrument response. Proceedings of the AIAA Conference on Sensor Systems for the 80's, Colorado Springs, Colorado, 2-4 December, pp. 76-83.

Duggin, M.J., Sakhavat, H. and Lindsay, J., 1985, Systematic and random variations in thematic mapper digital radiance data, Photogramm. Engrg. and Remote Sensing, 51, 1427.

Duggin, M.J., Lindsay, J. and Sakhavat, H., 1985, The systematic and random variation of feature vectors in a thematic mapper image, Internat. Jol. Remote Sensing, 6, 1257.

Duggin, M.J., 1985a, Factors limiting the discrimination and quantification of terrestrial features using remotely sensed radiance, Internat. Jol. Remote Sensing, 6, 3.

Duggin, M.J., 1985b, Comments on the intercalibration of multisensor, multitemporal, multichannel digital radiance data, Applied Optics, 24, 2292.

Egbert, D.D., and Ulaby, F.T., 1972, Effects of angles on reflectivity. Photogramm. Engng., 38, 556.

Forshaw, M.R.B., Haskell, A., Miller, P.F., Stanley, D.J. and Townshend, J.R.G., 1983, "Spatial resolution of remotely sensed imagery: a review paper", Int. J. Remote Sensing 4, 497.

Jackson, R.D., 1981, Interactions between canopy geometry and thermal infrared measurements. Proceedings of the Conference on Signatures Spectrales D'objets en teledetection. Avignon, 8-11 September, g.II. 5.291.

Kaneko, T., and Engvall, J.L., 1977, View angle effect in Landsat imagery. Proceedings of the 11th International Symposium on Remote Sensing of the Environment, Ann Arbor, Michigan, 945-951.

Kimes, D.S., 1981a, Azimuthal radiometric temperature measurements of wheat canopies. Appl. Optics, 20, 1119.

Kimes, D.S., 1981b, Remote sensing of temperature profiles in vegetation canopies using multiple view angles and inversion techniques. I.E.E.E. Trans. Geosci. Remote Sensing, 19, 85.

Kimes, D.S., 1983, Remote Sensing of row crops structure and component temperatures using directional radiometric temperatures and inversion techniques. Remote Sensing Environ., 13, 33.

Kimes, D.S., Idso, S.B., Pinter, P.J., Reginato, R.J., and Jackson, R.D., 1980, View angle effects in the radiometric measurement of plant canopy temperatures. Remote Sensing Environ., 10, 273.

Kimes, D.S. and Kirchner, J.A., 1983, Directional radiometric measurements of row-crop temperatures. Int. J. Remote Sensing, 4, 299.

Kirchner, J.A., and Schnetzler, C.C., 1981, Simulated directional radiances of vegetation from satellite platforms. Int. J. Remote Sensing, 2, 253.

Kieffer, H.H., Cook, D.A., Eliason, E.M. and Eliason, P.T., 1985. Intraband radiometric performance of the Landsat thematic mappers. Photogramm. Engrg. and Remote Sensing. 51. 1331.

Kollenkark, J.C., Vanderbilt, V.C., Daughtry, C.S.T. and Bauer, M.E., 1982. Influence of solar illumination angle on soybean canopy reflectance. Applied Optics 21. 1179.

Malila, W.A., Metzler, M.D., Rice, D.P. and Crist, E.P., 1984. Characterization of Landsat-4 MSS and TM digital image data. IEEE Trans. on Geoscience and Remote Sensing. GE-22. 177.

Markham, B.L. and Barker, J.L., 1985. Spectral characterization of the Landsat thematic mapper sensors. NASA Conference Publication 2355. Vol. 2. pp. 235-276.

Malaret, E., Bartolucci, L.A., Lozano, D.F., Anuta, P.E. and McGillem, C.D., 1985. Landsat-4 and Landsat-5 thematic mapper data quality analysis. Photogramm. Engrg. and Remote Sensing. 51. 1407.

Metzler, M. and Malila, W.A., 1985. Characterization and comparison of Landsat-4 and Landsat-5 thematic mapper data. Photogramm. Engrg. and Remote Sensing, 51, 1315.

Murphy, J.M., Ahern, F., Duff, P.F., and Fitzgerald, A.J., 1985, Assessment of radiometric accuracy of Landsat-4 and Landsat-5 thematic mapper data products from Canadian production systems. Photogramm. Engrg. and Remote Sensing. 51. 1359.

NASA, 1983, Interface Control Document between the NASA Goddard Space Flight Center (GSFC) and the Department of Interior, EROS Data Center (EDC) for Landsat-D Thematic Mapper Computer Compatible Tape (CCT-AT, CCT-PT) Revision A, NASA Document LSD-1CD-105.

Poros, D.J. and Peterson, C.J., 1985, Methods for destriping Landsat thematic mapper images - a feasibility study for an online destriping process in the thematic mapper imaging system (TIPS). Photogramm. Engrg. and Remote Sensing, 51, 1371.

Schott, J. and Volchok, W.J., 1985, Thematic mapper thermal infrared calibration. Photogramm. Engrg. and Remote Sensing, 51, 1351.

Schowengerdt, R.A., Archwamety, C. and Wrigley, R.C., 1985, Landsat thematic mapper image-derived MTF, Photogramm. Engrg. and Remote Sensing, 51, 1395.

Schnetzler, C.C., 1981, Effect of sun and sensor geometry, canopy structure and density and atmospheric conditions on the spectral response of vegetation, with particular emphasis on across-track pointing. Proceedings of the Conference on Signatures Spectrales d'objets en teledetection, Avignon, 8-11 September, pp. 509-520.

Singh, A., 1985, Postlaunch corrections for thematic mapper 5 (TM-5) radiometry in the thematic mapper image processing system (TIPS). Photogramm. Engrg. and Remote Sensing, 51, 1385.

Slater, P.N., 1979, A re-examination of the Landsat MSS. Photogramm. Engng. Remote Sensing, 45, 1479.

Smith, J.A., 1979, MRS Literature Survey of Bidirectional Reflectance. ORI Inc., 1400 Spring Rd., Silver Spring, Maryland.

Smith, J.A., 1983, in Manual of Remote Sensing, Vol. 1, 2nd ed., Amer. Soc. of Photogrammetry, Falls Church, VA.

Suits, G.H., and Safir, G., 1972, Verification of a reflectance model for mature corn with applications to corn blight detections. Remote Sensing Environ. 2, 183.

Tilton, J.C., Markham, B.L. and Alford, W.L., 1985, Landsat-4 and Landsat-5 MSS coherent noise: characterization and removal. Photogramm. Engrg. and Remote Sensing, 51, 1263.

Turner, R.E., 1978, Elimination of atmospheric effects from sensor data. Proceedings of the 12th International Symposium on Remote Sensing of the Environment, Ann Arbor, Michigan, pp. 1651-1697.

U.S. Geological Survey, 1979, Landsat Data Users Handbook, U.S. Geological Survey, Washington, D.C.

U.S. Geological Survey, 1984, Landsat 4 Data Users Handbook, U.S. Geological Survey, and National Oceans and Atmospheric Association, Washington, D.C.

Wardley, N., 1984, Vegetation index variability as a function of viewing geometry, Int. J. Remote Sensing, 5, 861.

Wrigley, R.C., Card, D.H., Hlavka, C.A., Hall, J.A., Mertz, F.C., Archwamety and Schowengerdt, R.A., 1984, Thematic mapper image quality: registration, noise and resolution, IEEE Trans on Geoscience and Remote Sensing, GE-22, 263.

Wrigley, R.C., Hlavka, C.A. and Card, D.H., 1985, Evaluation of thematic mapper interband registration and noise characteristics. Photogramm. Engrg. and Remote Sensing, 51, 1417.

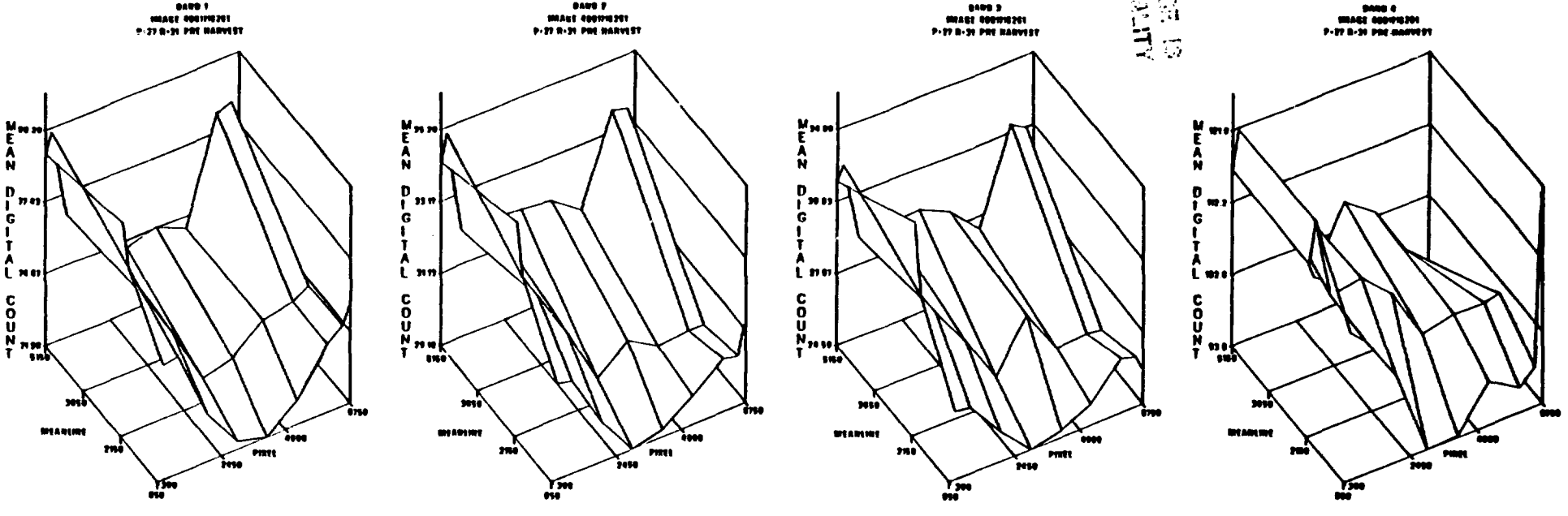

Fig. 1

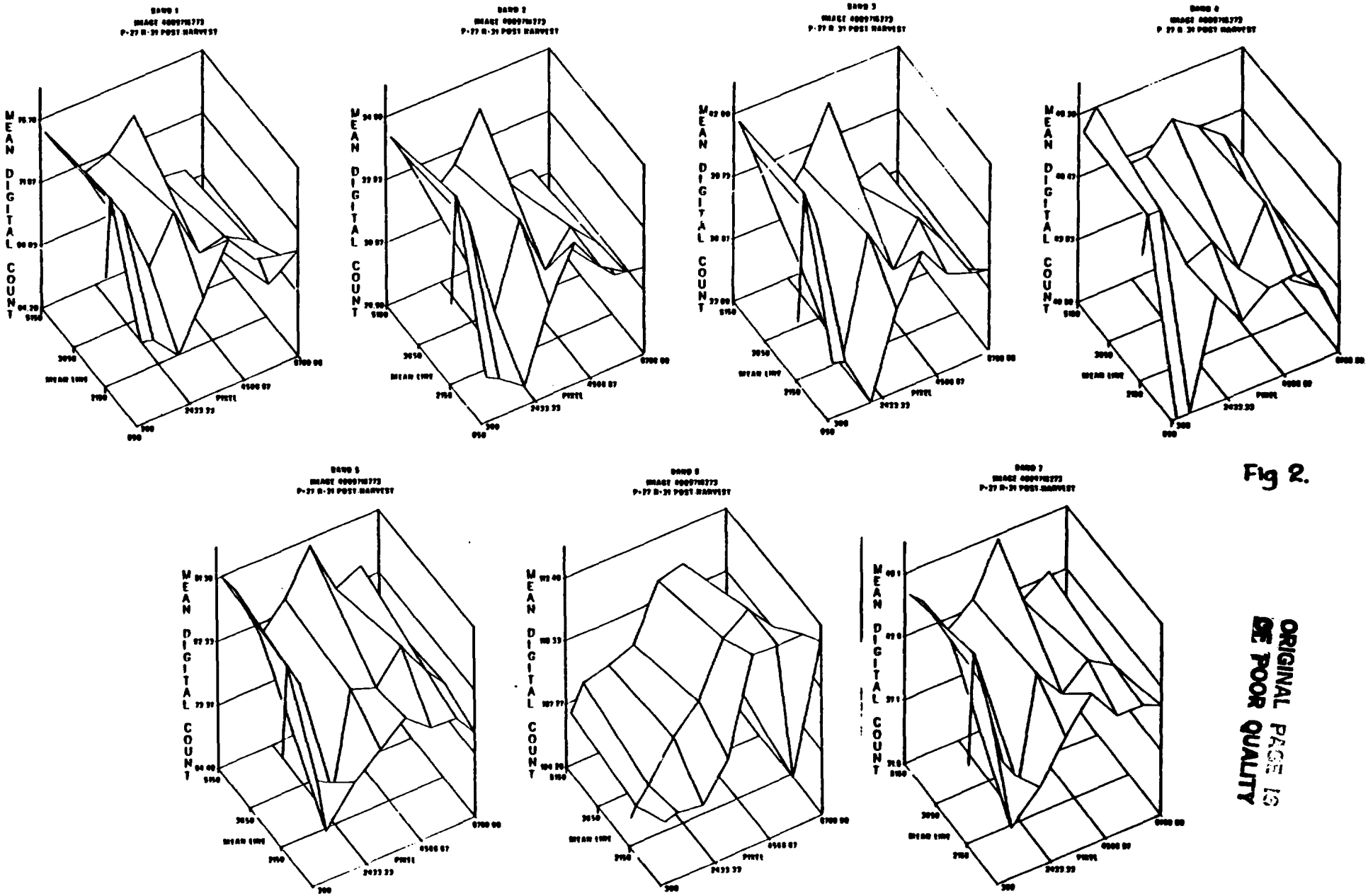

Fig 2.

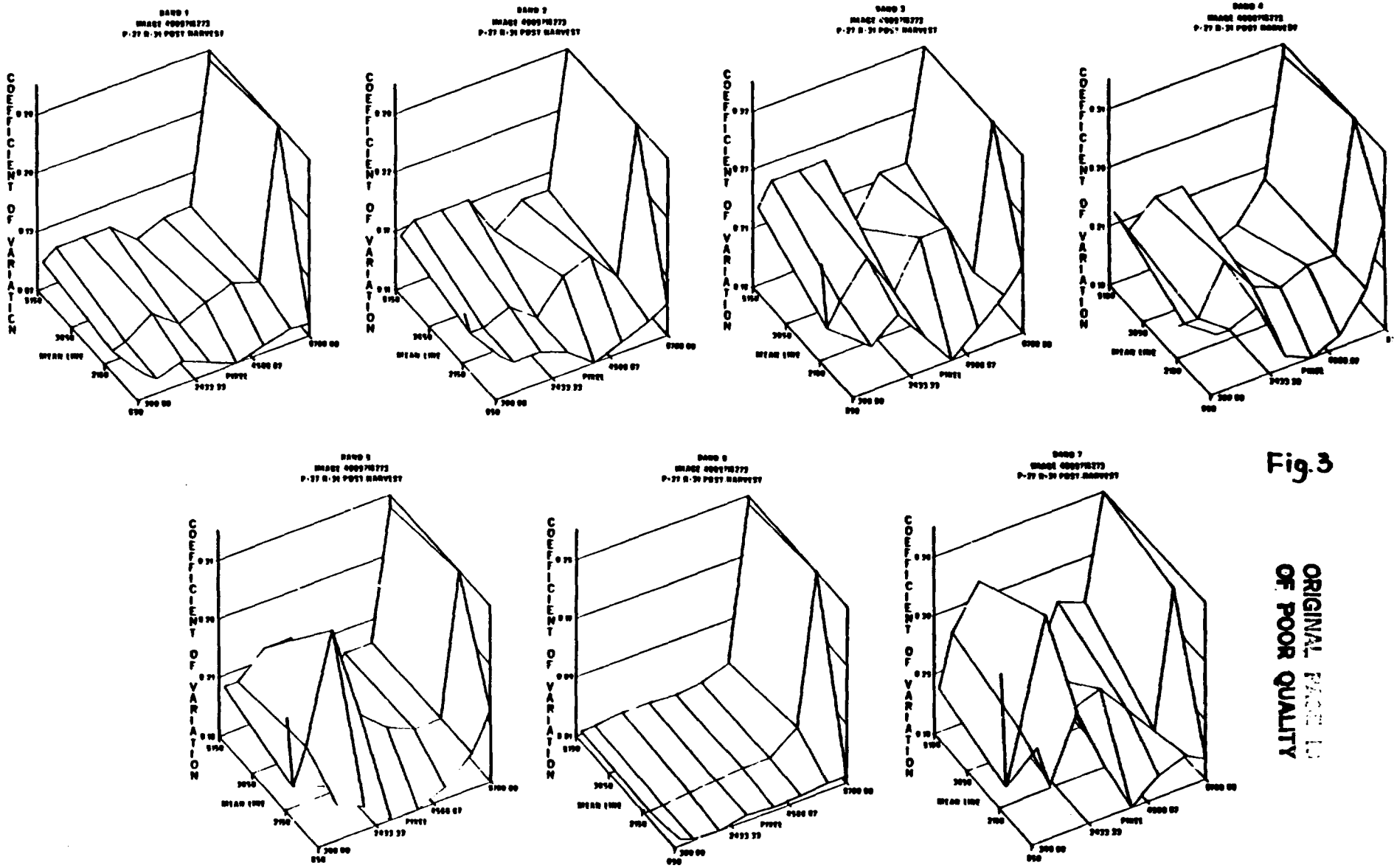

Fig. 3

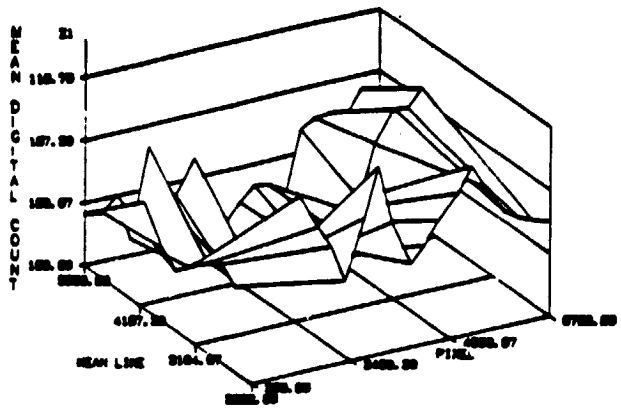

BAND 3
IMAGE 5016716293 AUG. 15 1984
P=27 R=31 PRE-HARVEST

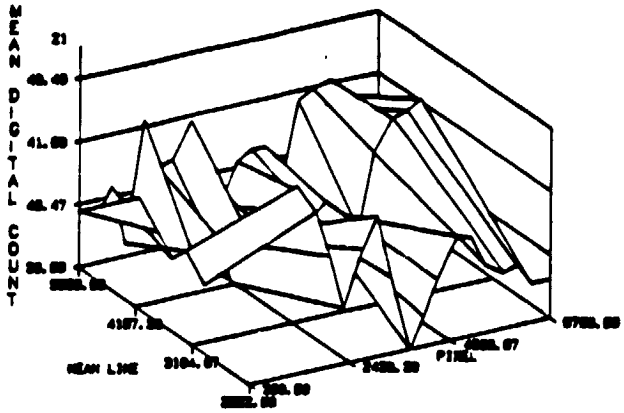

BAND 4
IMAGE 5016716293 AUG. 15 1984
P=27 R=31 PRE-HARVEST

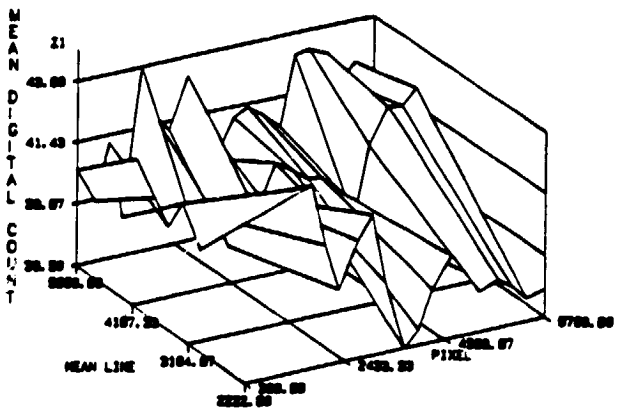

BAND 5
IMAGE 5016716293 AUG. 15 1984
P=27 R=31 PRE-HARVEST

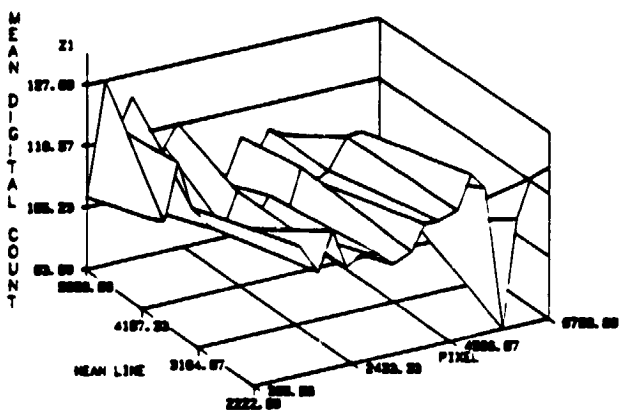

BAND 6
IMAGE 5016716293 AUG. 15 1984
P=27 R=31 PRE-HARVEST

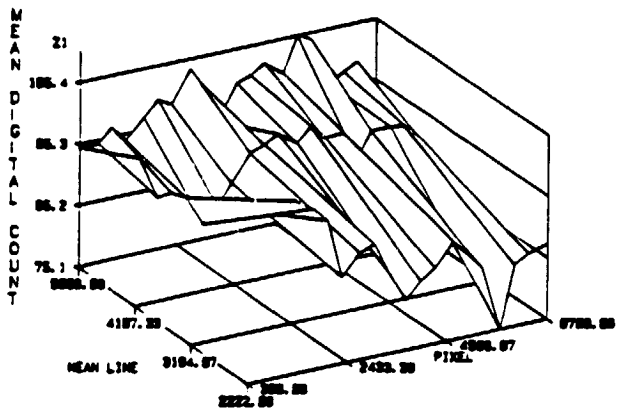

BAND 7
IMAGE 5016716293 AUG. 15 1984
P=27 R=31 PRE-HARVEST

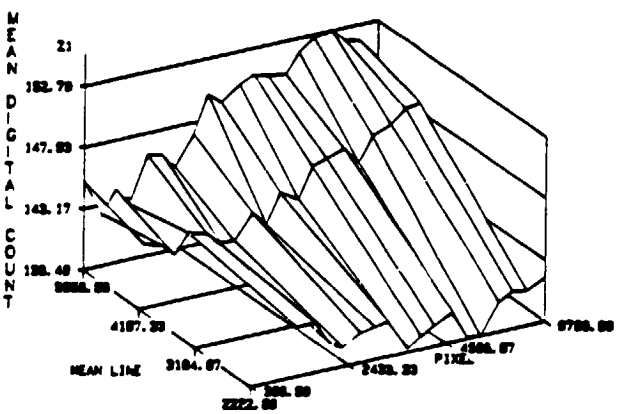

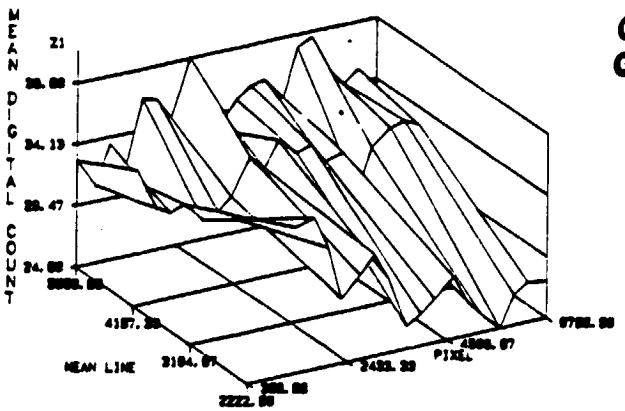

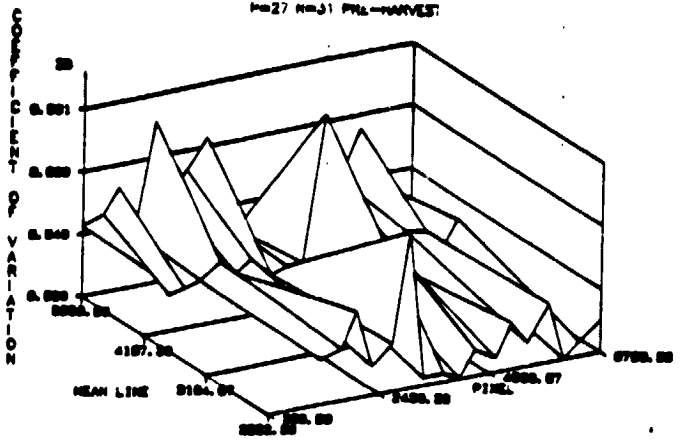

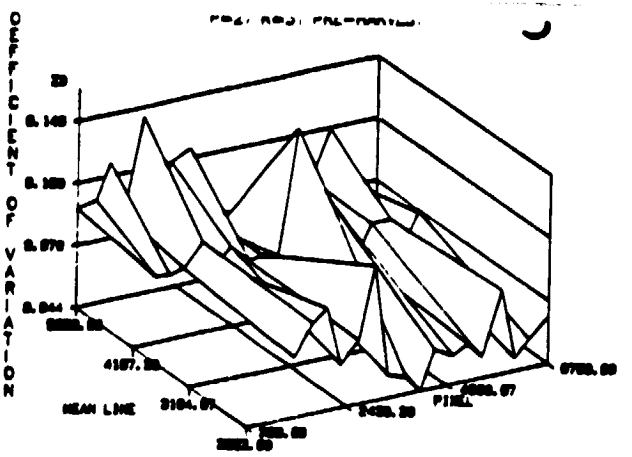

BAND 3
IMAGE 5016716293 AUG. 15 1984
P=27 R=31 PRE-HARVEST

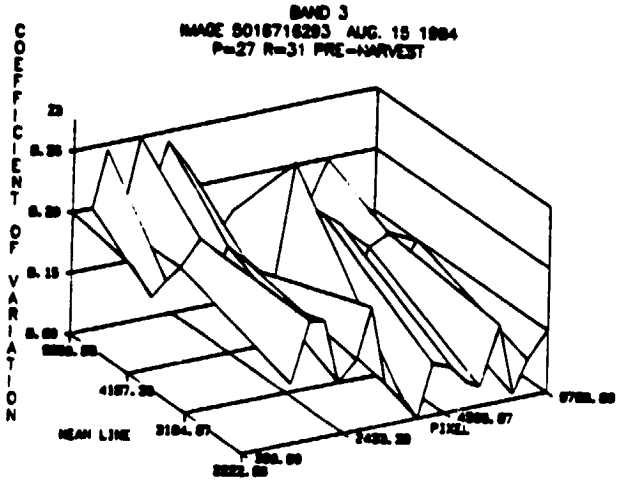

BAND 4
IMAGE 5016716293 AUG. 15 1984
P=27 R=31 PRE-HARVEST

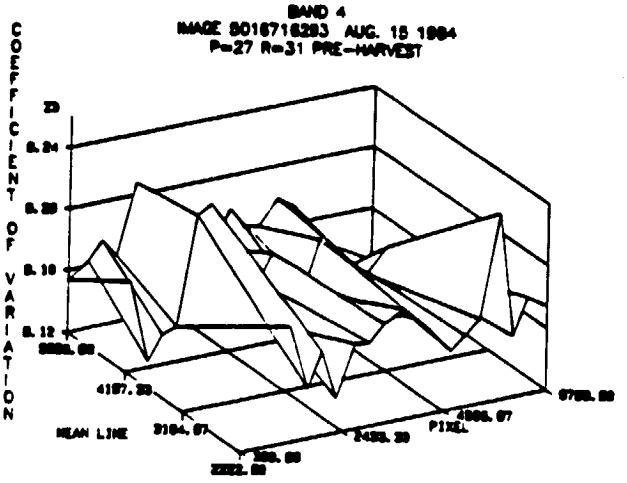

BAND 5
IMAGE 5016716293 AUG. 15 1984
P=27 R=31 PRE-HARVEST

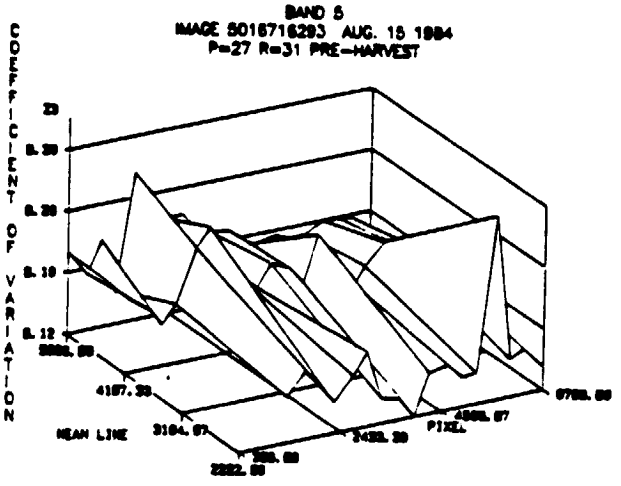

BAND 6
IMAGE 5016716293 AUG. 15 1984
P=27 R=31 PRE-HARVEST

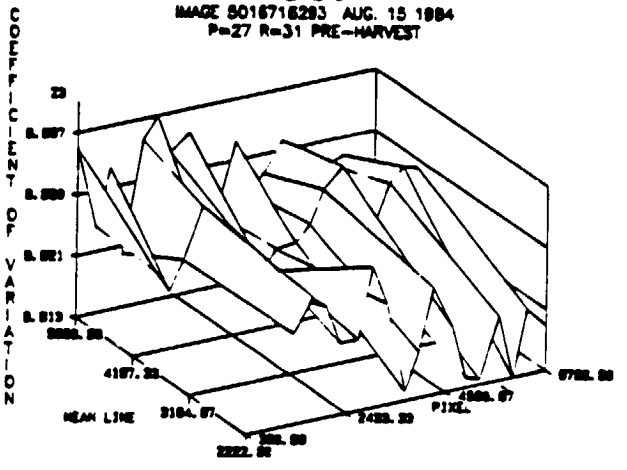

BAND 7
IMAGE 5016716293 AUG. 15 1984
P=27 R=31 PRE-HARVEST

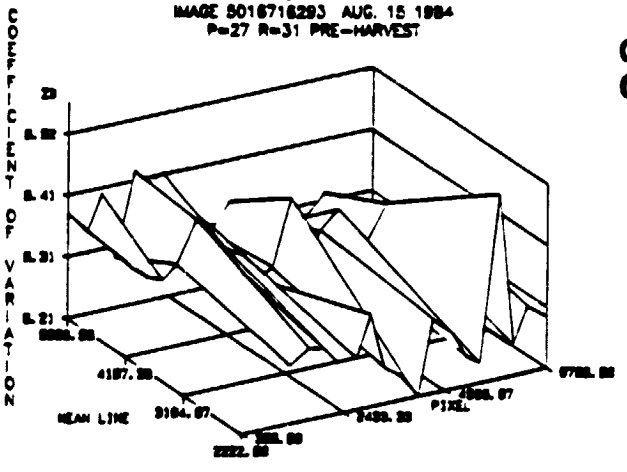

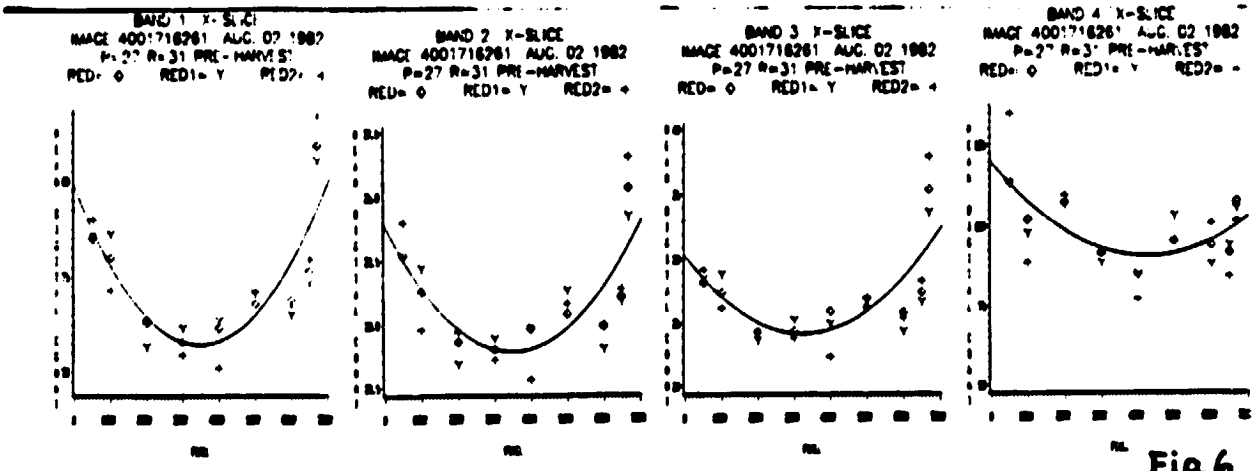

Fig. 6

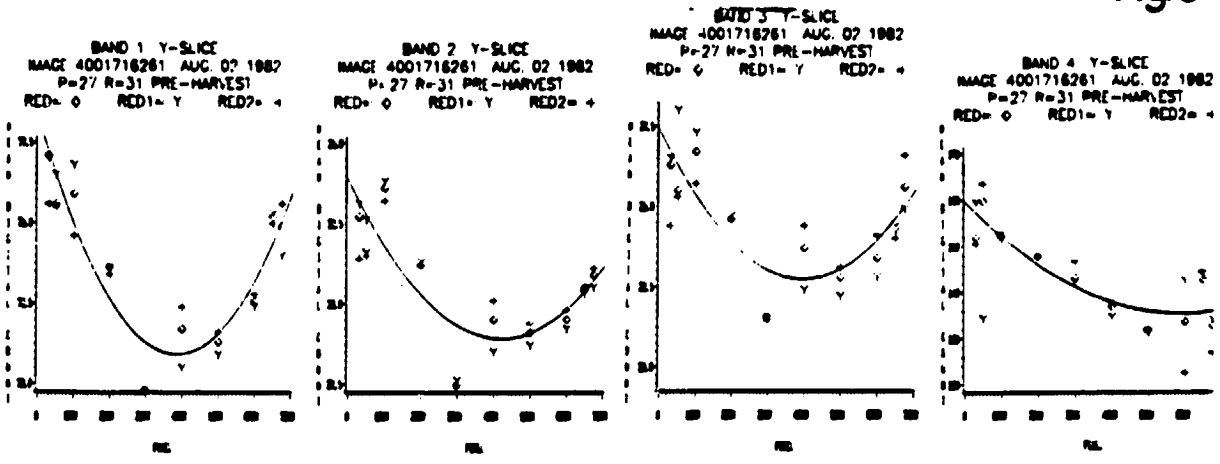

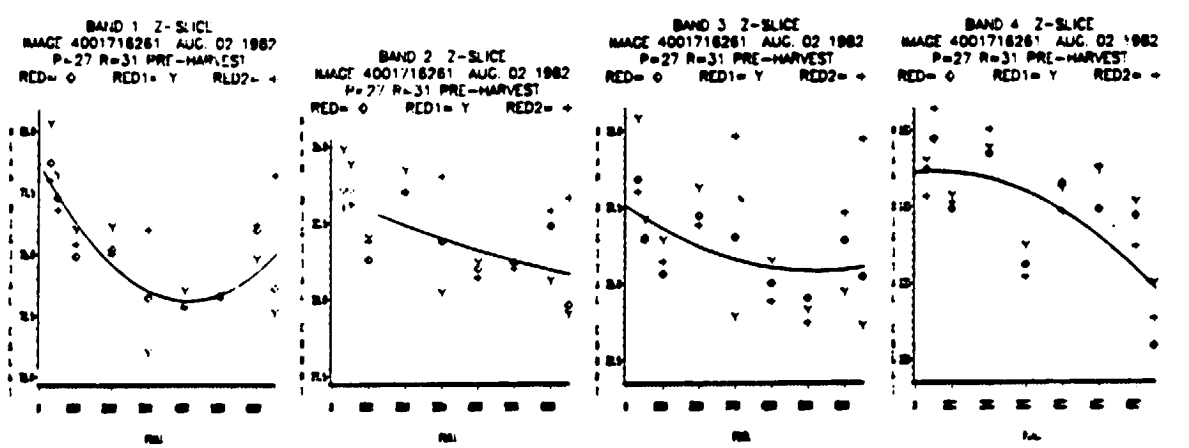

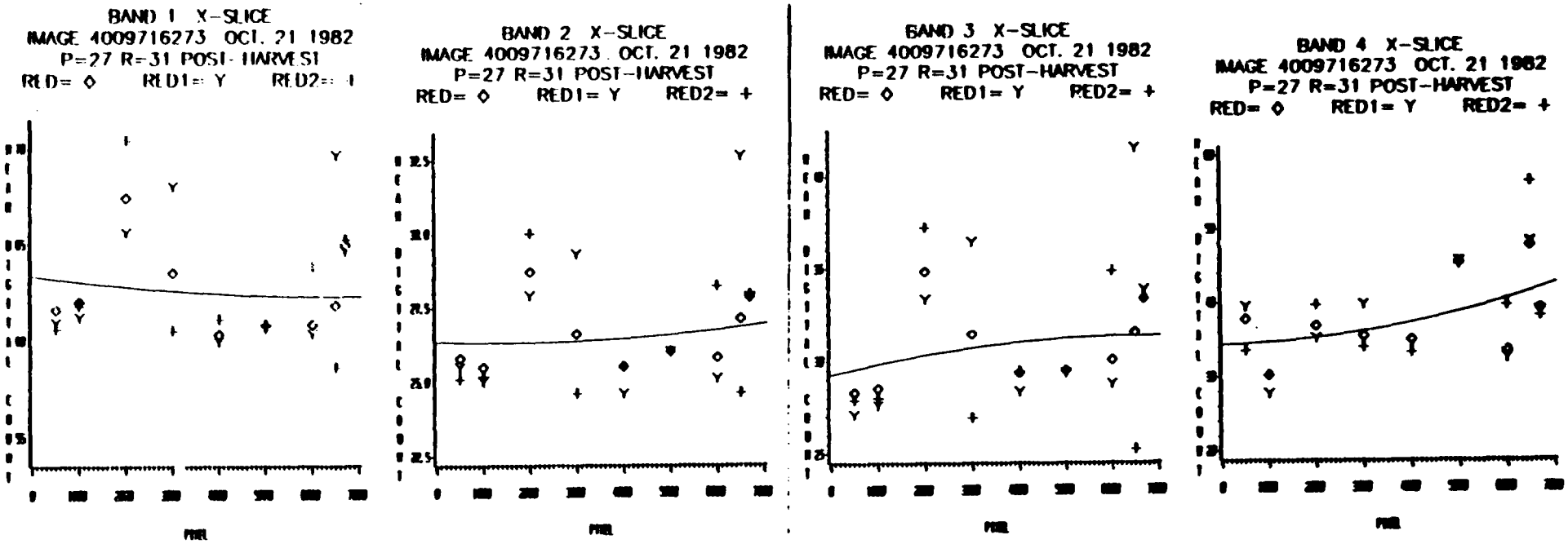

Fig. 7

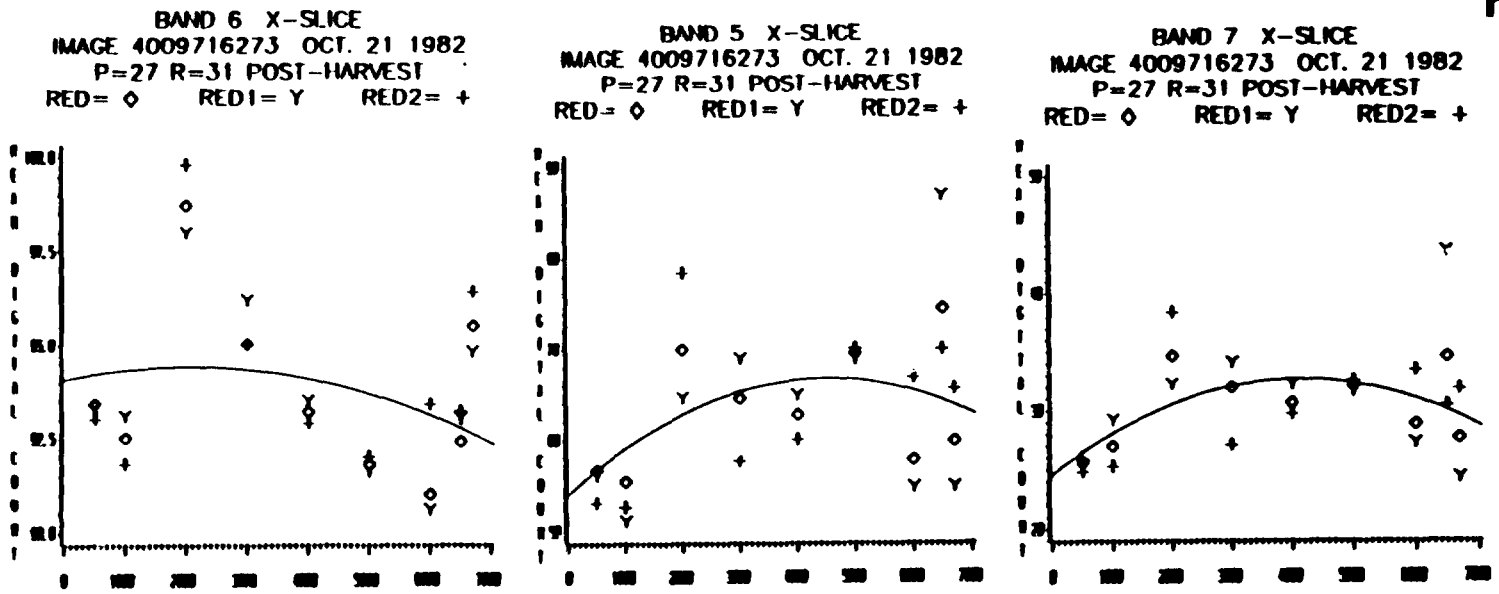

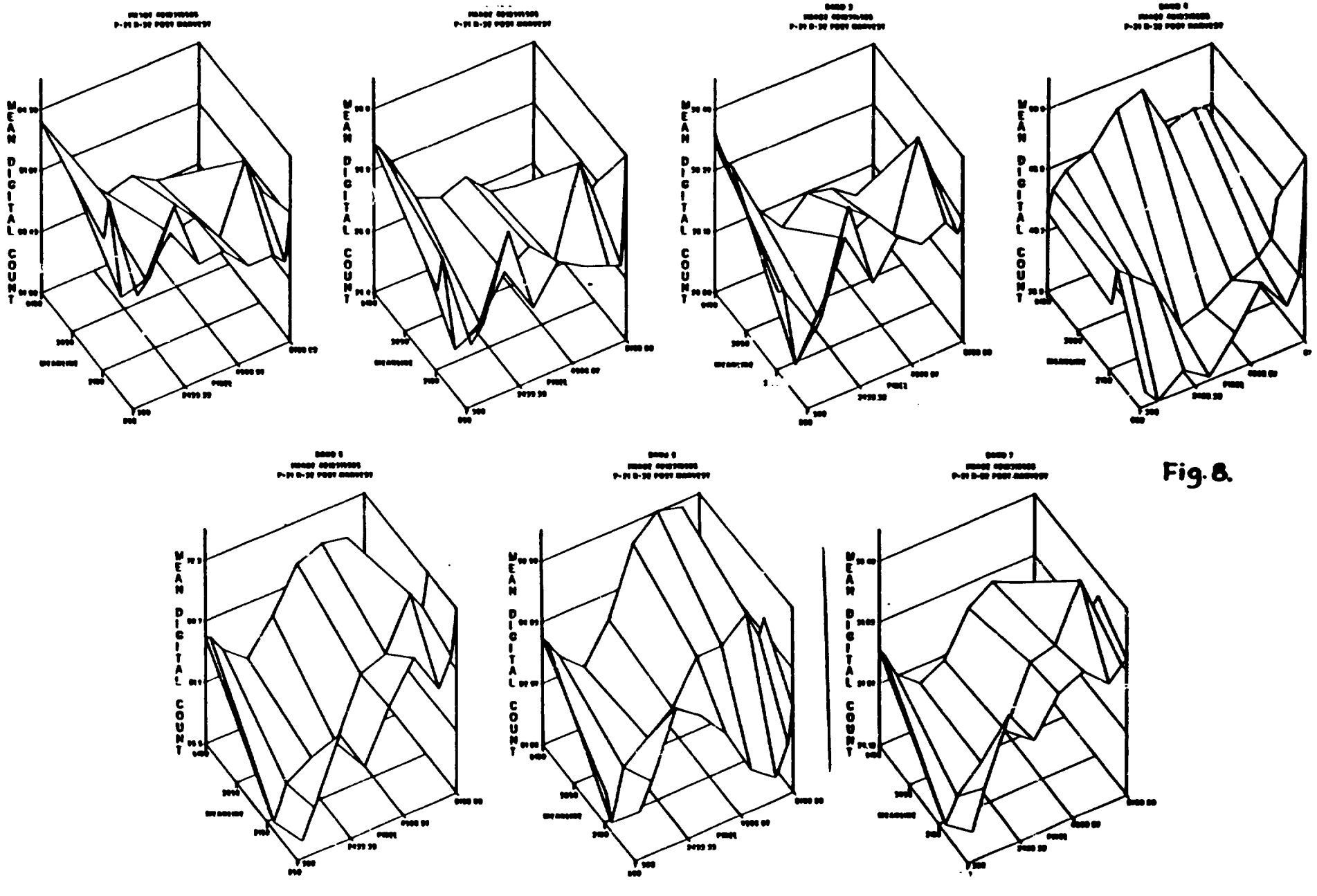
MEAN DIGITAL COUNT
MEAN DIGITAL COUNT
MEAN DIGITAL COUNT
MEAN DIGITAL COUNT
MEAN DIGITAL COUNT
MEAN DIGITAL COUNT
MEAN DIGITAL COUNT

Fig. 8.

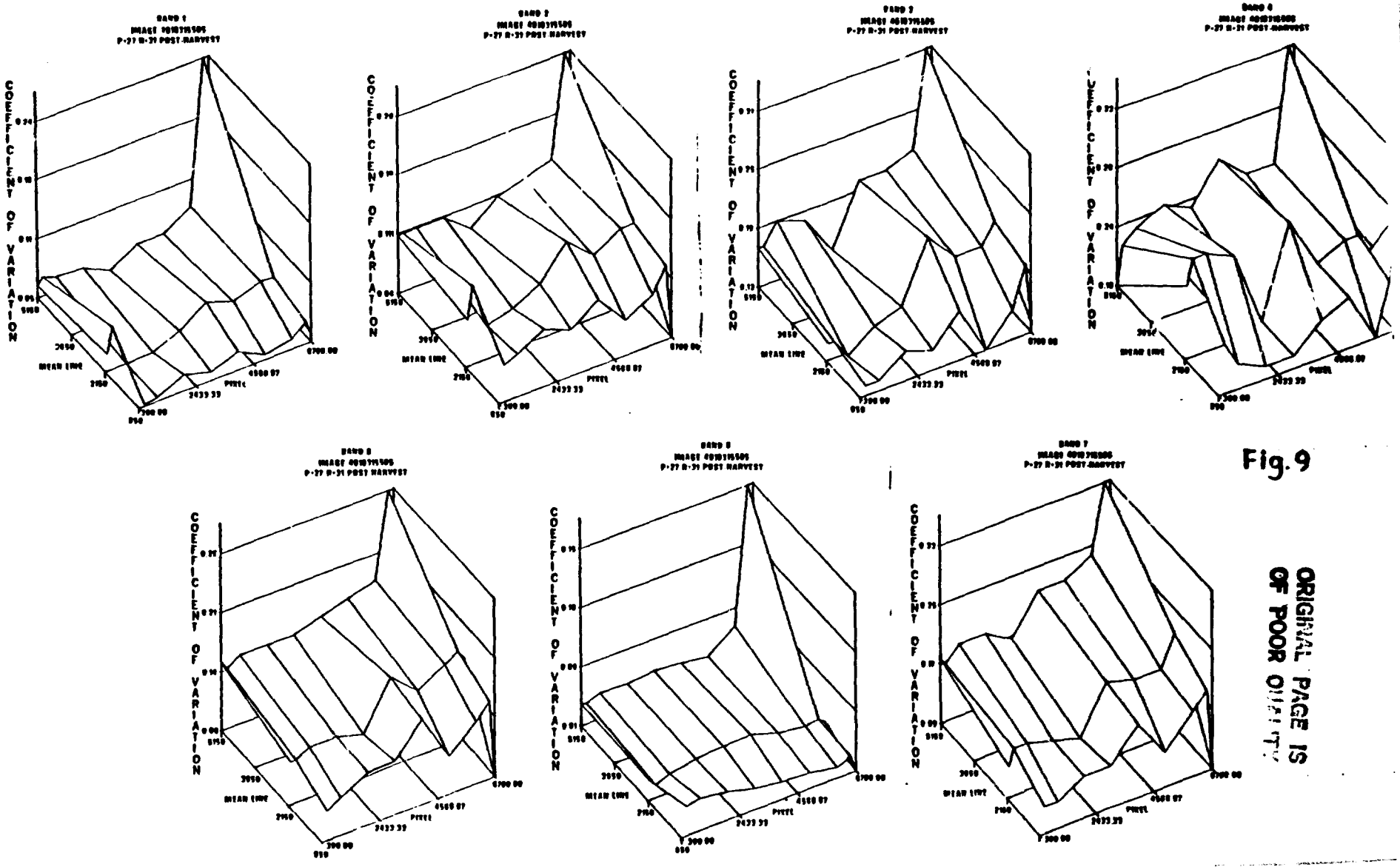

Fig. 9

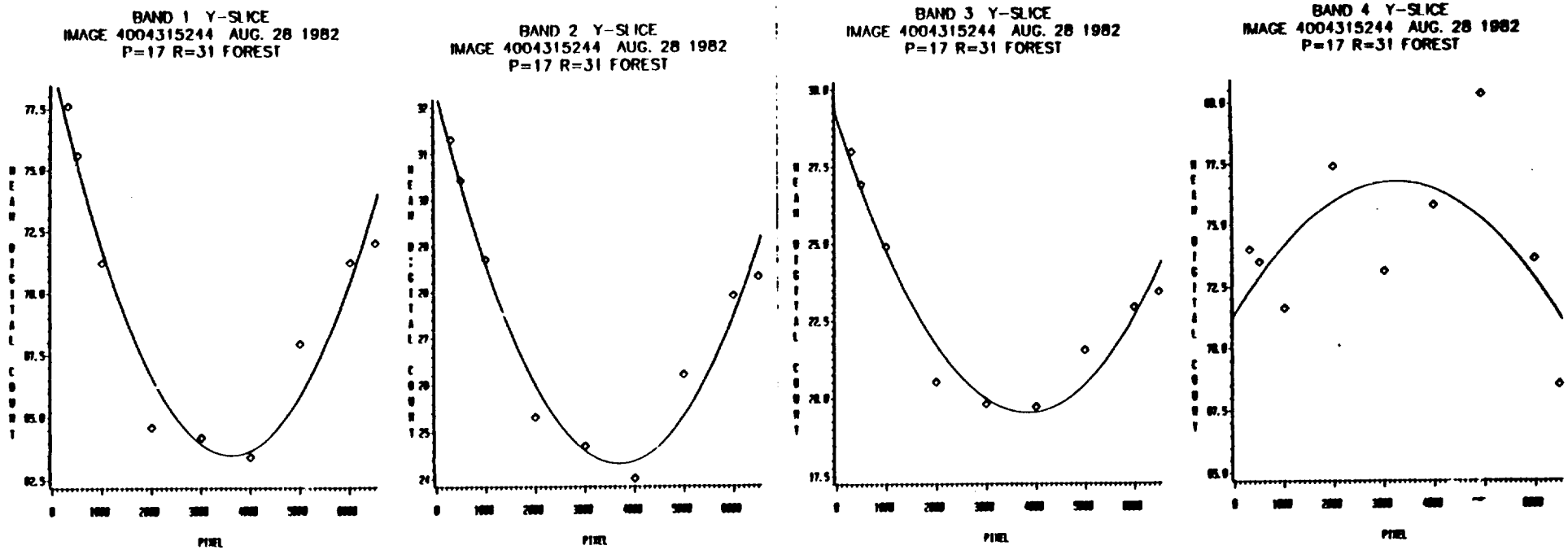
BAND 1 Y-SLICE
IMAGE 4004315244 AUG. 28 1982
P=17 R=31 FOREST
BAND 2 Y-SLICE
IMAGE 4004315244 AUG. 28 1982
P=17 R=31 FOREST
BAND 3 Y-SLICE
IMAGE 4004315244 AUG. 28 1982
P=17 R=31 FOREST
BAND 4 Y-SLICE
IMAGE 4004315244 AUG. 28 1982
P=17 R=31 FOREST
PIXEL

Fig.10

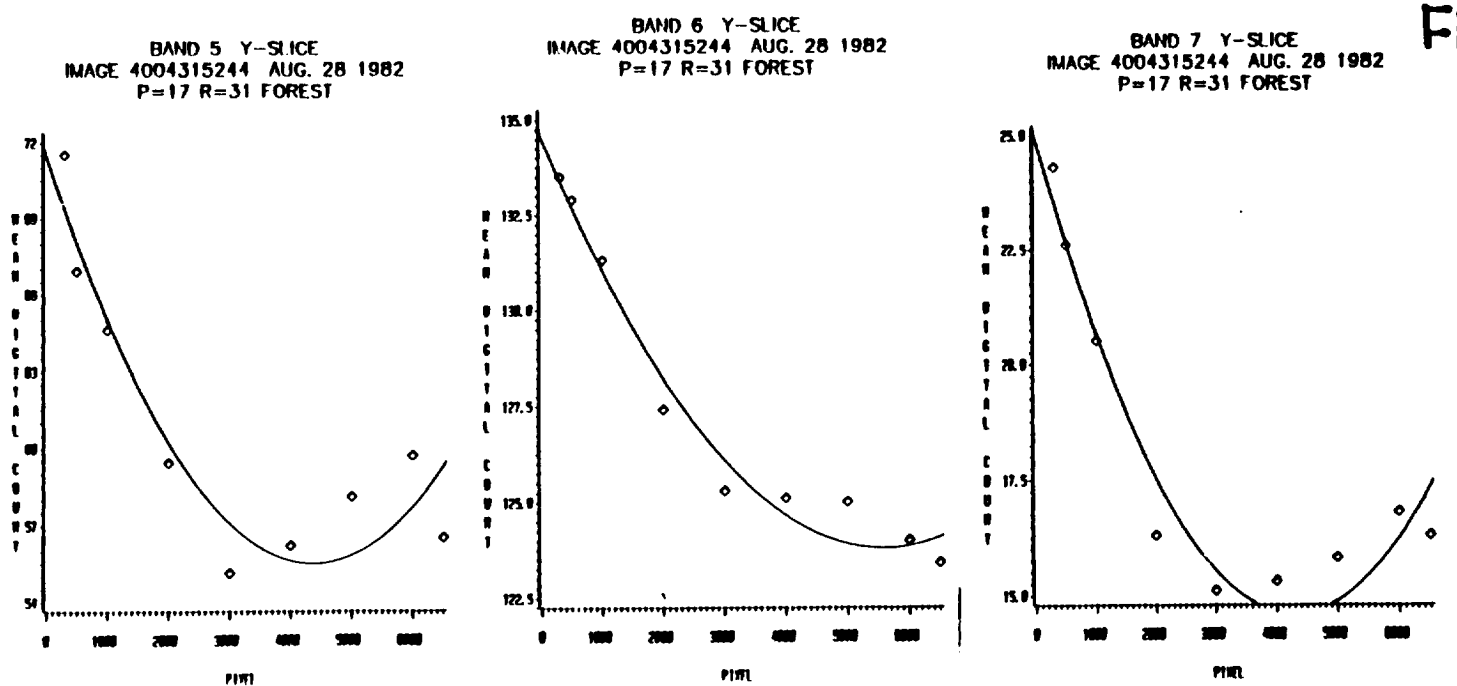
BAND 5 Y-SLICE
IMAGE 4004315244 AUG. 28 1982
P=17 R=31 FOREST
BAND 6 Y-SLICE
IMAGE 4004315244 AUG. 28 1982
P=17 R=31 FOREST
BAND 7 Y-SLICE
IMAGE 4004315244 AUG. 28 1982
P=17 R=31 FOREST
PIXEL

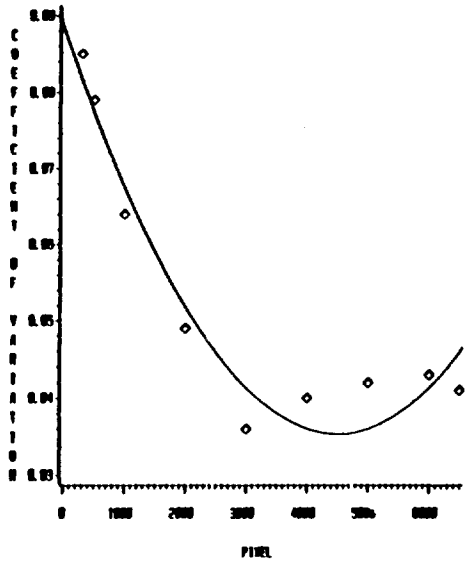

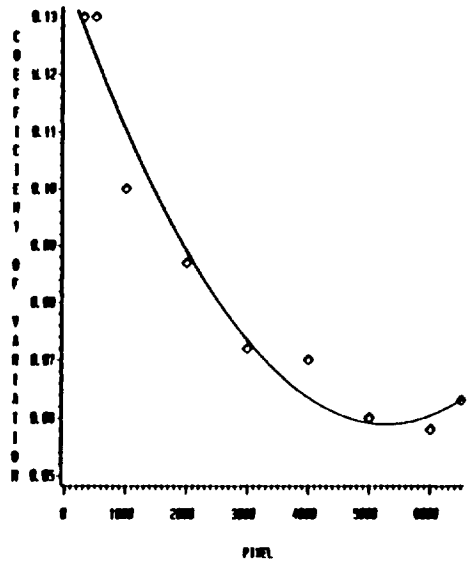

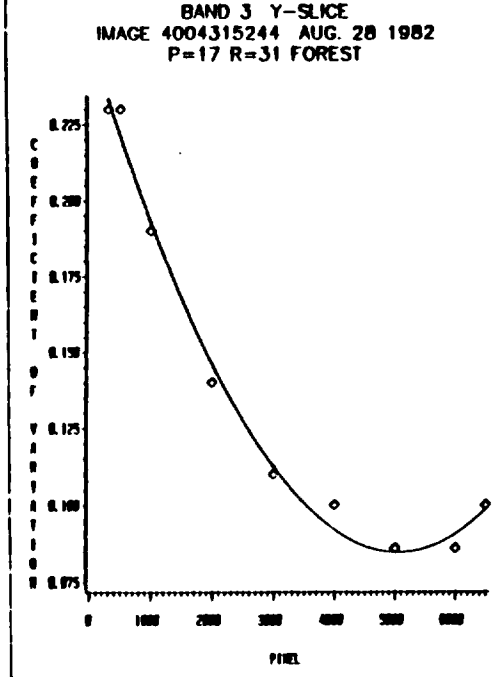

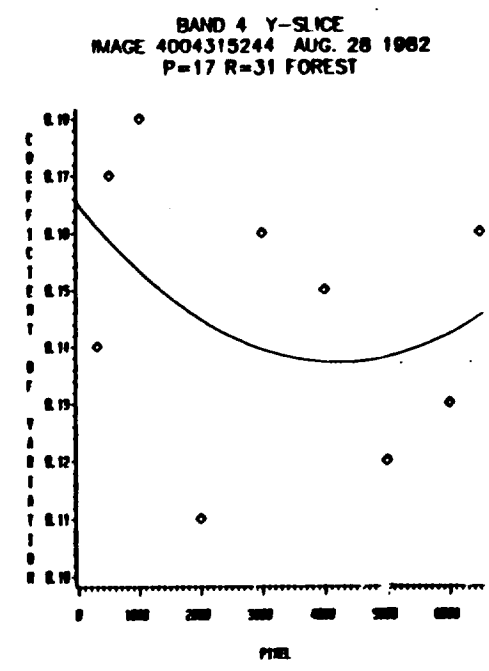

Fig. 11

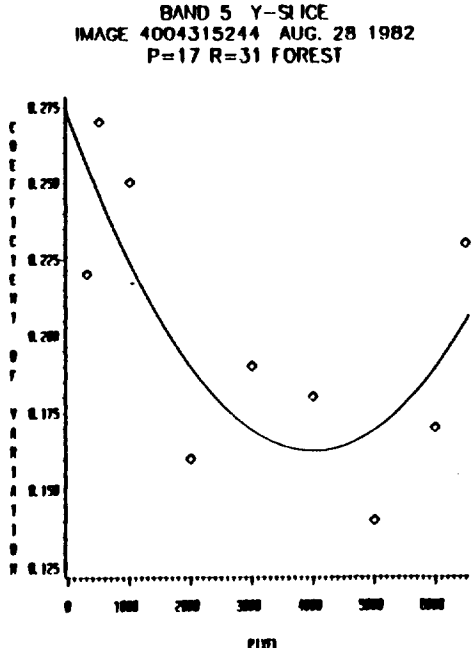

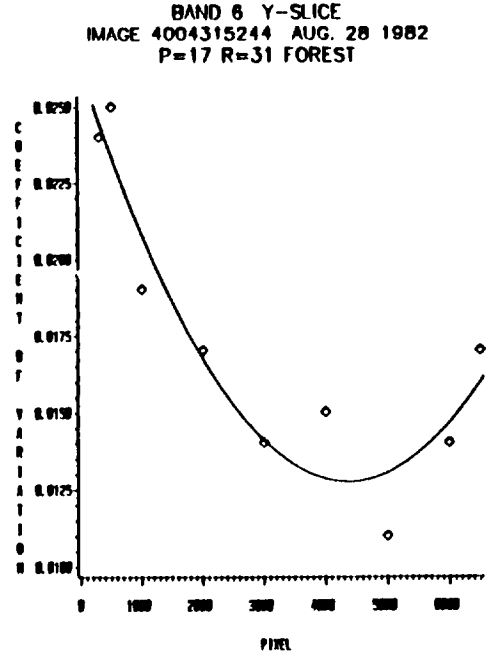

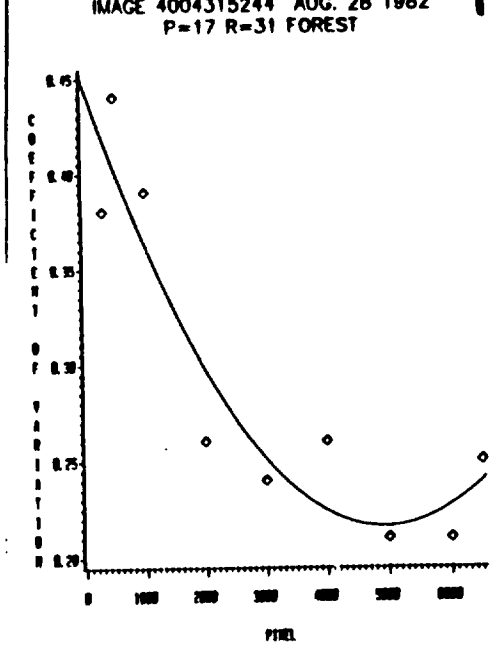

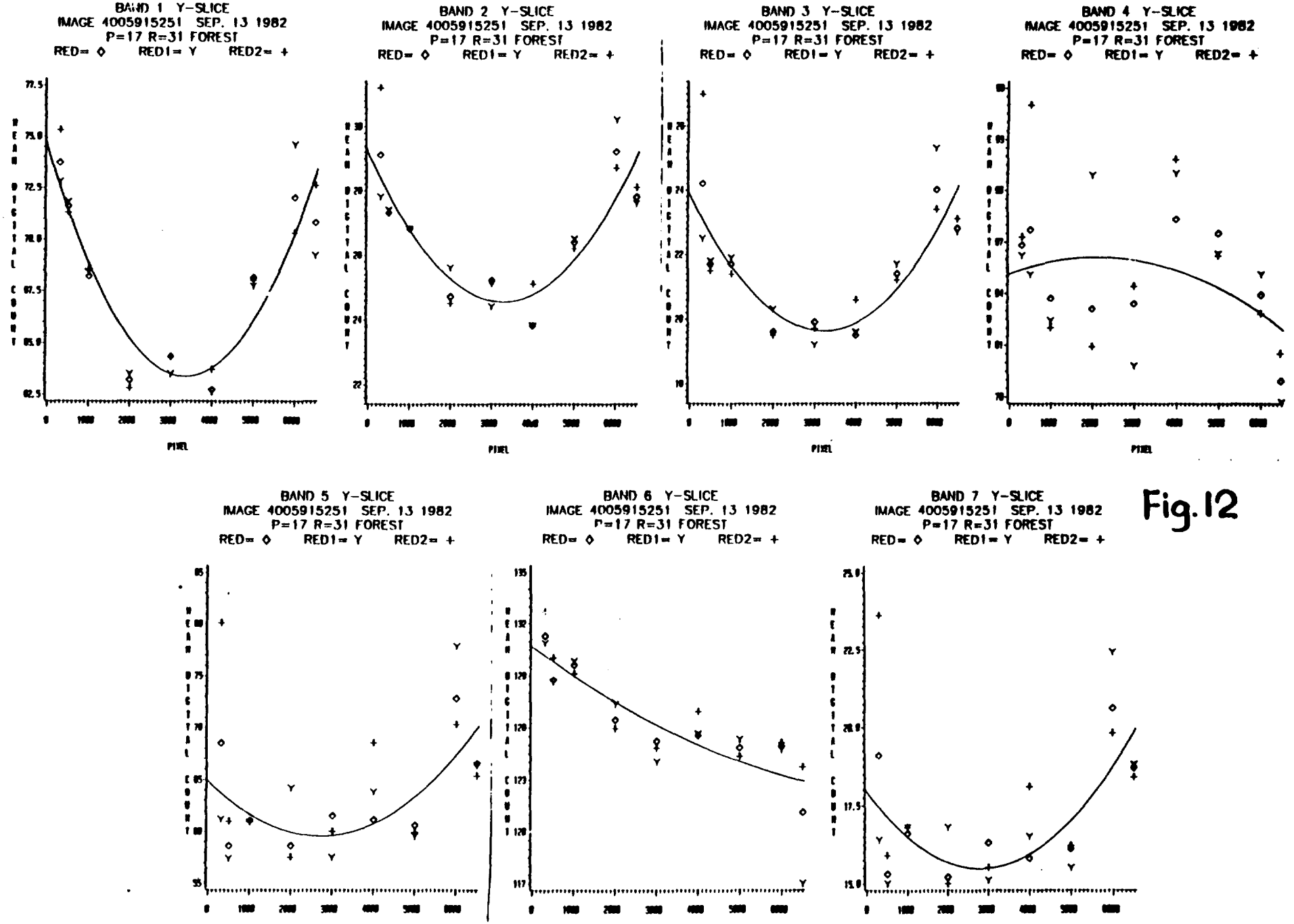
BAND 1 Y-SLICE
IMAGE 4005915251 SEP. 13 1982
P=17 R=31 FOREST
RED= ◇ RED1= Y RED2= +
BAND 2 Y-SLICE
IMAGE 4005915251 SEP. 13 1982
P=17 R=31 FOREST
RED= ◇ RED1= Y RED2= +
BAND 3 Y-SLICE
IMAGE 4005915251 SEP. 13 1982
P=17 R=31 FOREST
RED= ◇ RED1= Y RED2= +
BAND 4 Y-SLICE
IMAGE 4005915251 SEP. 13 1982
P=17 R=31 FOREST
RED= ◇ RED1= Y RED2= +
BAND 5 Y-SLICE
IMAGE 4005915251 SEP. 13 1982
P=17 R=31 FOREST
RED= ◇ RED1= Y RED2= +
BAND 6 Y-SLICE
IMAGE 4005915251 SEP. 13 1982
P=17 R=31 FOREST
RED= ◇ RED1= Y RED2= +
BAND 7 Y-SLICE
IMAGE 4005915251 SEP. 13 1982
P=17 R=31 FOREST
RED= ◇ RED1= Y RED2= +

Fig. 12

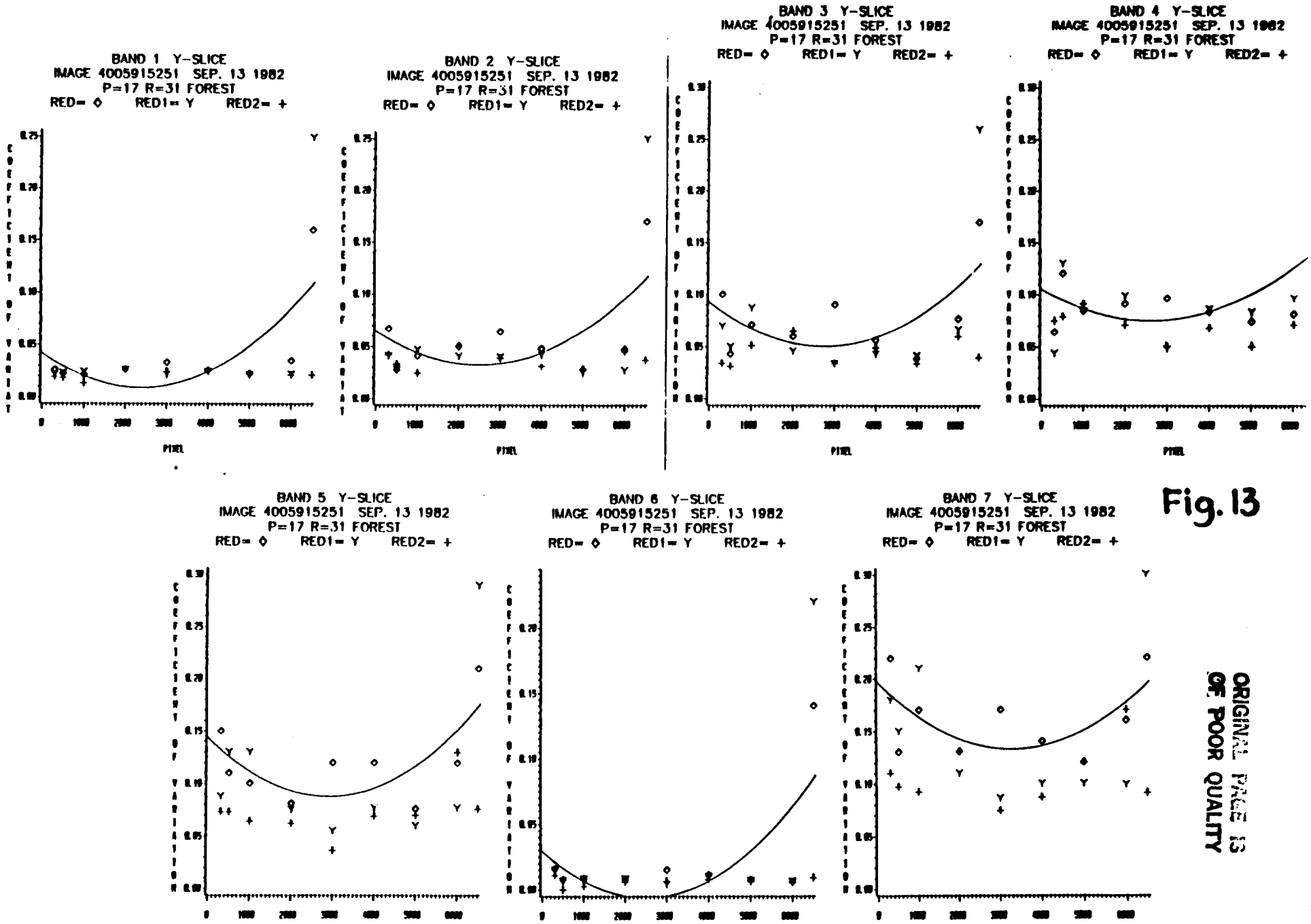

Fig. 13

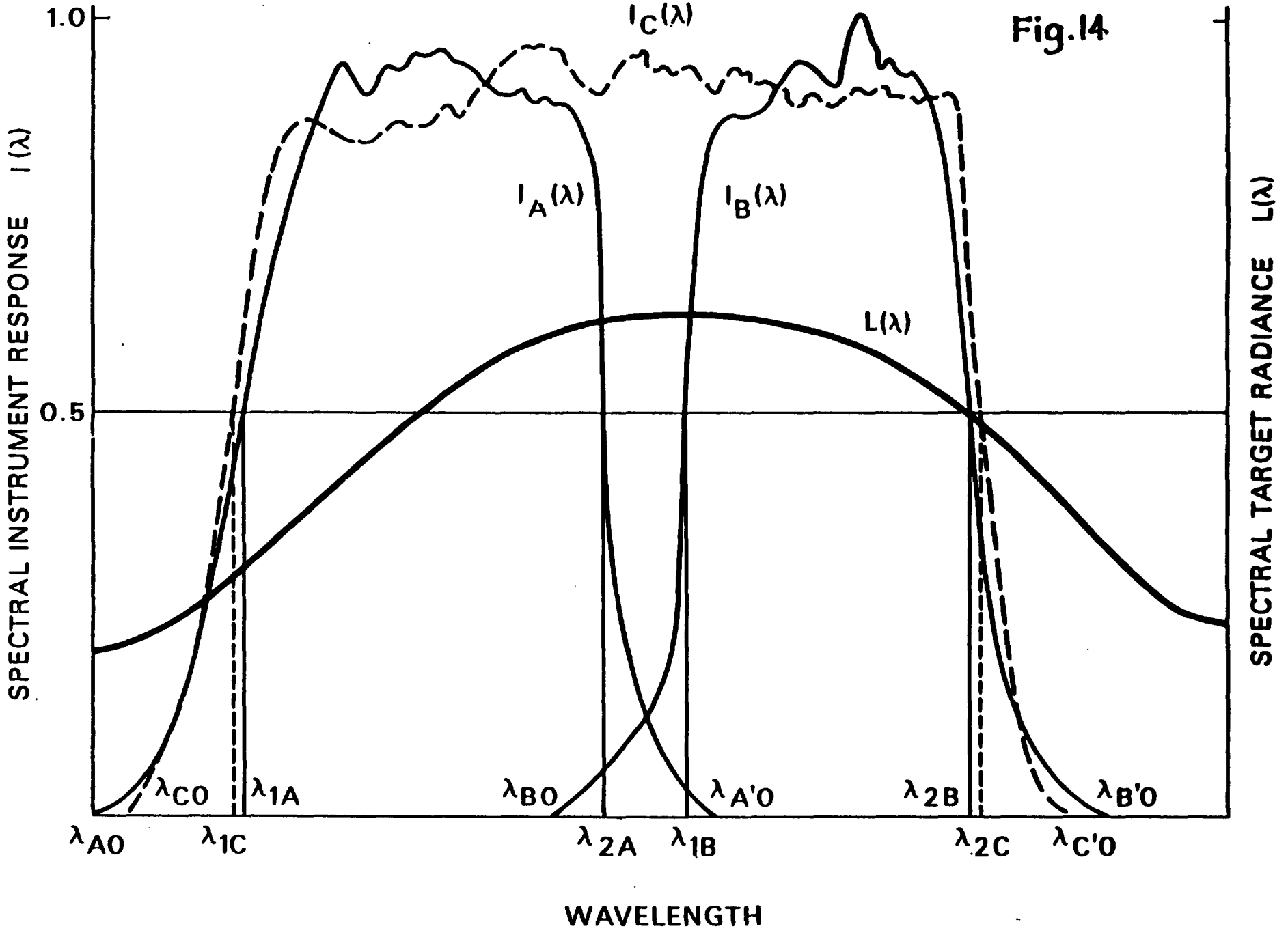
Fig.14
1.0
0.5
$I_C(\lambda)$
$I_A(\lambda)$
$I_B(\lambda)$
$L(\lambda)$
SPECTRAL INSTRUMENT RESPONSE $I(\lambda)$
SPECTRAL TARGET RADIANCE $L(\lambda)$
λ_{C0}
λ_{1A}
λ_{B0}
$\lambda_{A'0}$
λ_{2B}
$\lambda_{B'0}$
λ_{A0}
λ_{1C}
λ_{2A}
λ_{1B}
λ_{2C}
$\lambda_{C'0}$
WAVELENGTH

Fig. 15

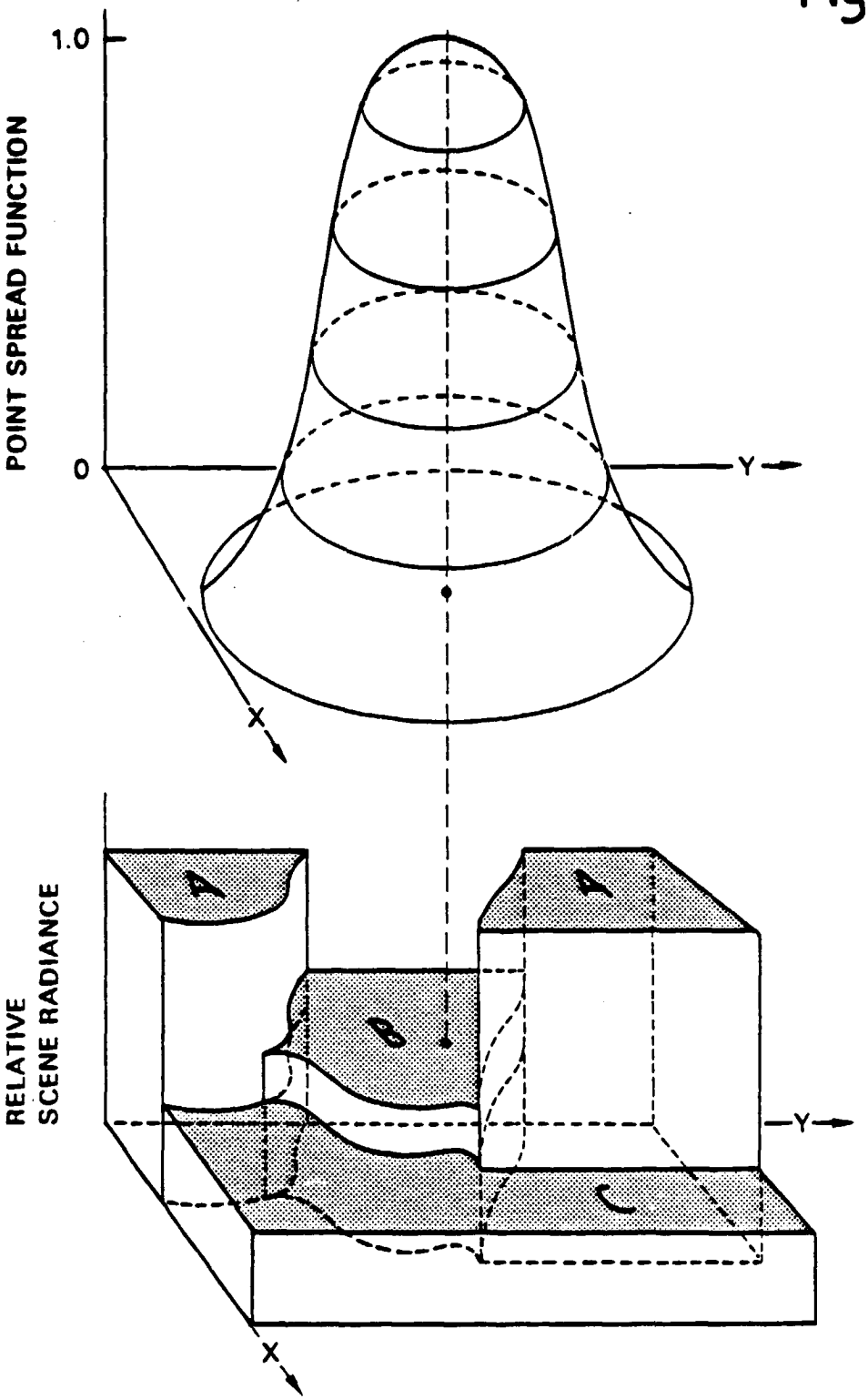
1.0
POINT SPREAD FUNCTION
0
Y
X
RELATIVE
SCENE RADIANCE
A
A
B
C
Y
X

APPENDIX A
THE USE OF MULTIDATE MULTICHANNEL RADIANCE DATA IN URBAN FEATURE ANALYSIS

M.J. Duggin*, R. Rowntree+, M. Emmons**, N. Hubbard++, A.W. Odell+++, M. Sakhavat* and J. Lindsay***

*308 Bray Hall

SUNY - College of Environmental Science and Forestry

Syracuse, NY 13210, USA

+Northeastern Experiment Station

U.S. Forest Service

State University of New York

Syracuse, NY 13210, USA

**Mail Code 636
Goddard Space Flight Center, NASA

Greenbelt, MD 20771, USA

++ERSAC Ltd.

Peel House, Ladywell,

Livingston, West Lothian,

Scotland EH546AG, U.K.

+++Space Department

Royal Aircraft Establishment

Farnborough

Hants GU146TD, ENGLAND

***Systems and Applied Science Corporation

1572 Spring Hill Road

Vienna, VA 22180, USA

ABSTRACT

Previous work has suggested that seasonally varying reflectance properties are predictably related to radiance recorded by multichannel remote sensing devices. Two images were obtained from thematic mappers on Landsats 4 and 5 over the Washington, D.C. area during November 1982 and March 1984. These were registered and selected training areas containing different types of urban land use were examined, one area consisting entirely of forest. Mean digital radiance values for each bandpass, in each image were examined and variances, standard deviations and covariances between bandpasses were calculated. We found that two bandpasses caused forested areas to stand out from other land use types, especially for the November 1982 image. In order to evaluate quantitatively the possible utility of principal components analysis in selected feature extraction, the eigenvectors were evaluated for principal axes rotations which rendered each selected land use type most separable from all other land use types. The evaluated eigenvectors were plotted as a function of land use type, whose order was decided by considering anticipated shadow component and by examination of the relative loadings indicative of vegetation for each of the principal components for the different features considered. The analysis was performed for each seven-band image separately and for the two combined images. We found that by combining the two images, we obtained more dramatic land use type separation. Conclusions have been drawn from this preliminary work suggesting directions for further study. Both British and U.S. image analysis systems were used.

INTRODUCTION

Thematic mapper (TM) data have a nominal spatial resolution of 29m in all bandpasses except the thermal infrared band. The TM potentially has utility for measurements of urban land use and of vegetation configuration within land use types (e.g. Quattrochi 1983, Haack 1983, Forster 1983, Jensen, et al 1983). Registered, multidate images of TM data each contain 7 bands of data. There is promise of superior feature identification and of urban forest identification using principal components analysis of TM digital multiband radiance data (e.g., Bernstein, et al 1984) or other transformations (e.g., Crist and Cicone, 1984) to reduce the dimensionality of the data without reducing its information content. This approach has been discussed frequently (e.g., Stiteler 1979) and will facilitate data reduction. Such considerations are important in economical data analysis and in the representation of mapped features using images formed from only three primary colors.

In this report, we discuss the results of an experiment to show that principal components analysis may be used to effectively distinguish between different urban land cover classes and that this may be done more effectively by using a combination of images obtained on two different dates than by using either of the images individually. In order to quantify the superiority of using combined (superimposed) images, we have chosen to evaluate the eigenvectors for selected test areas, showing that the magnitudes of the eigenvectors are most different for the combination of images obtained on two dates than for either of the individual images, in the cases of those principal components explaining most of the variance in the data.

ANALYSIS AND DISCUSSION OF RESULTS

In this preliminary experiment we utilized two registered TM images obtained over the Washington, D.C. area (November 2nd, 1982 and March 24, 1984). The former image was obtained by Landsat 4 (image no. 4010915140) and the latter was obtained by Landsat 5 (image no. 5002315112). We registered these images on the Landsat Assessment System at NASA, Goddard Space Flight Center. The superimposed 512 pixel by 512 Line extracts were then output to tape and subsequently were interactively analyzed by using the GEMS interactive image analysis sytem located at the Royal Aircraft Establishment, Farnborough, England, and also by using the GEMS interactive image analysis system at ERSAC, Ltd. in Edinburgh, Scotland. The individual images are shown in Fig. 1. A linear stretch has been applied to each image.

Four training sites were selected as "typical" and are shown outlined in the lower center image in Fig. 2. These consisted of "Forest", "Dense urban", "Downtown" and "Airport". The forest area has a 100% canopy cover, and is to the northwest of the city. The downtown area includes the park areas which contain few trees but extensive lawns, including those between the Lincoln Memorial and the House of Congress. The dense urban area has virtually no trees and is to the east of the downtown area and Washington National Airport is included as the fourth area, being a mix of concrete, buildings and grass, the last being less well maintained than that in the area between the Lincoln Memorial and the House of Congress. These four areas are annotated on the image at the bottom center of Fig. 2. The training sites contained the following numbers of pixels.

Forest	7480
Dense urban	5852
Airport	2448
Downtown	9246

These sample sizes were sufficiently large to perform a reliable analysis.

We have shown the mean radiance values recorded for each of the four land use categories used in the study in Table 1. In this table, we have ordered the land use categories in terms of decreasing vegetation conteNt. TM band 4 (0.76-0.90 m) shows a decreasing value with decreasing vegetation for both images, although the downtown area does appear to show approximately the same band 4 radiance value as forest in March 1984. This would seem reasonable, since deciduous trees are not in leaf in March, and will give rise to lower band and radiance values. TM band 6 (10.4-12.5 m) shows the thermal radiance recorded from the training areas increasing with decreasing vegetation content. Again the distinctions are most consistent in November 1982. A ratio of (TM band 6/TM band 4) shows an increasing value with decreasing vegetation content. This suggests that TM imagery could be useful in mapping vegetation, especially in mapping forest in urban environments.

The principal components transformation was performed by using training areas (Fig. 2) over selected land use types, so as to rotate the measurement axes (i.e., axes describing recorded radiance in each band) to make the selected land use type most separable from "everything else". The eigenvectors were evaluated for each of the four selected land use types identified in the training sites after principal components analysis was performed to emphasize that feature. Similar calculations were performed, but without training, for the whole 512 pixel x 512 line image extract: the 14 principal component images for the two superimposed images are shown in Fig. 3. The eigenvalues for the first three principal components were such as to explain generally over ninety percent of the variation in the data. The eigenvectors have also been calculated for each image and for the fourteen band composite obtained by combining the two seven band images: in this case the first seven bands consisted of those from one image and the latter seven bands (in the same sequence) contained digital

radiance data from the second image. The evaluated eigen vectors are shown in Table 2.

Fig. 4 shows a plot of the eigenvectors for the first principal component for each date, for axis rotations performed to emphasize land use types in each training area and for the whole image extract. The eigenvectors for the second and third principal components show less difference between land use types categorized by the training sites for the combined or for the single-date images. However, in each case, there is a substantial difference between each of the eigenvectors for a given principal component and the eigenvector for the same principal component for the whole image. This demonstrates the separability of each land use type using this technique.

Fig. 5 shows the percentage of variation in the data explained by each principal component for the fourteen band image. This is the only image so illustrated, for reasons of space. Fig. 6 shows the loadings (scaled to the range 1.0) of each of the components (feature vectors) in the eigenvector for each principal component calculated to emphasize the four features contained in training areas considered for the two images (fourteen band) composite. The forest area clearly has considerable shadow and a low albedo and thus has a lower eigenvector (first principal component) than that of the dense urban area, which is less than that of the airport, which in turn is less than that of the downtown area. Note that the loadings of the components (measurement vectors) for each of the training sites shows a progressive change from forest to downtown area. It is suggested that both shadow and the vegetative component contained in the training area contribute to the differences in loadings. It is noted that the loadings for the bandpasses of the March 1984 images generally exceed (in modulus) those for the November 1982 image. The seasonal vegetational change and the change in shadow component due to the change in solar azimuth and zenith angles at the time of satellite overpass will also be

important in contributing to new information in the second image which was not present in the first. This explains why the first principal component calculated for the composite fourteen band image was superior in separating the features contained within the training areas identified earlier on and shown in Fig. 2.

It is suggested that either a canonical variate formed from the evaluated eigenvectors obtained by training on a class containing a land use category or possibly the principal components of ratioed images might be worth investigating as better land use type discriminators. Clearly, these possibilities need to be investigated and the intercalibration between the digital radiance data from the Landsat 4 and 5 thematic sensors needs to be taken into account (e.g. Duggin 1985, Likens and Wrigley 1985, Palmer 1984).

CONCLUSION

A feasibility study involving the principal components analysis performed by training upon selected urban land use types to make them most separable from other imaged features has been described for single-date and for registered multidate images. It appears that separability is enhanced by using the increased spectral radiance information contained in superimposed images obtained on different dates. It appears probable that shadow and vegetation vigor, as well as changes in these parameters are important in controlling feature separability. It appears that TM bands 4 and 6 contain information which best discriminates forest from other areas and which may therefore be of use in urban forest studies. Further work on a larger suite of images, containing a larger variety of urban forest land use patterns is underway.

ACKNOWLEDGEMENTS

This work was partly supported by U.S. Forest Service cooperative agreement 23-850, work unit NE-1952, partly by NASA Contract NAS-27595. We benefited from the goodwill and help of colleagues at NASA Goddard Space Flight Center, the Royal Aircraft Establishment, Farnborough and ERSAC, Ltd. We would also like to thank G.C. Stone for his helpful comments and encouragement. Constructive suggestions by C.J. Robinove and J. Estes are also appreciated.

TABLE CAPTION

Table 1. Mean radiance values for each training site (land use category) for each image studied.

Table 2. Calculated eigenvectors for the principal components obtained by training on selected features, to so rotate the axes as to enhance the separability of those features selected and by calculating the principal components axis rotation for the whole image. Values are shown for the first three principal components for each of the two images and for the fourteen band superimposed image pair.

FIGURE CAPTIONS

Fig. 1. Single band extracts of images superimposed Landsat thematic mapper (512 pixels x 512 lines) obtained on two dates; 2 November 1982 (Landsat 4) and 24 March 1984 (Landsat 5). The images are contrast enhanced by using a linear stretch.

Fig. 2. Training areas used in 512 x 512 pixel image.

Fig. 3. Principal components images obtained for the whole 512 pixel x 512 line extract of the fourteen band composite of the superimposed images. The training area (extracts) of the few selected cover types are also shown.

Fig. 4. Plot of the eigenvectors as a function of training site (Fig. 2) and for the whole 512 x 512 pixel image extraction for the first principal component for each of the images and for the composite of the two superimposed images.

Fig. 5. Plot of the percentage of variation in the data explained by each of the principal components for the fourteen band (composite) image. In each case the axes have been so rotated to as facilitate the extraction of the selected feature.

Fig. 6. Loadings (scaled to fall between 1.0) of the feature vectors in calculating the eigenvectors for the first three principal components when the axes are so rotated as to emphasize each of the selected features.

REFERENCES

Bernstein, R., Lotspiech, J.B., Meyers, H.J., Kolsky, H.G. and Lees, R.D., 1984, Analysis and processing of Landsat-4 sensor data using advanced image processing techniques and technologies, IEEE Transactions on Geoscience and Remote Sensing GE22, 192-221.

Crist, E.P. and Cicone, R.C., 1984, A physically-based transformation of thematic mapper data - the TM tasseled cap. IEEE Transactions on Geoscience and Remote Sensing GE22, 256-263.

Duggin, M.J., 1985, Comments on the intercalibration of multisensor, multitemporal multichannel digital radiance data; to appear in Applied Optics.

Forster, B.C., 1985, An examination of some problems and solutions in monitoring urban areas from satellite platforms. International J. Remote Sensing, 6, 139-151.

Haack, B.N., 1983, An analysis of thematic mapper simulator data for urban environments, Remote Sensing of Environment 13, 265-275.

Jensen, J.R., Bryan, M.L., Friedman, S.Z., Henderson, F.M., Holz, R.K., Lindgren, D., Toll, D.L., Welch, R.A., and Wray, J.R., 1983, Urban/suburban land use analysis. In Manual of Remote Sensing, Vol. 2, ed. by R.M. Colwell, pp. 1571-1666.

Likens, W.C. and Wrigley, R.C., 1985, Impact of Landsat MSS sensor differences on change detection analysis. Landsat-4 Science Characterization Early Results, NASA Conference Publication 2355, Vol. 1, pp. 159-176.

Palmer, J.M., 1984, Effective bandwidths for Landsat-4 and Landsat-D' multispectral scanner and thematic mapper subsystems, IEEE Transactions on Geoscience and Remote Sensing, GE22, pp. 336-338.

Quattrochi, D.A., 1983, An initial analysis of Landsat-4 thematic mapper data for the discrimination of agricultural, forested wetlands, and urban land cover. Landsat-4 Science Characterization Early Results, NASA Conference Publicatin 2355, Vol. 4, pp. 131-151.

Stiteler, W.M., 1979, Multivariate statistics with applications in statistical ecology, Multivariate Methods in Ecological Work, ed. Orleci, L., Rao, C.R. and Stiteler, W.M., International Cooperative Publishing House, Fairland, MD, pp. 229-300.

Table 1.

TM band	Forest		Airport		Downtown		Dense Urban	
	Nov. 82	March 84	Nov. 82	March 84	Nov. 82	March 84	Nov. 82	March 84
1	58.7	86.3	72.1	99.7	70.9	99.9	67.8	95.3
2	23.8	33.6	30.5	42.0	29.4	42.0	27.7	38.7
3	24.6	36.0	31.4	46.4	30.3	45.9	28.5	42.5
4	37.3	49.5	35.2	47.6	33.6	50.0	31.6	42.8
5	40.8	76.6	48.0	75.9	42.9	74.4	41.9	70.6
6	113.5	112.1	116.0	121.9	116.5	120.0	117.2	124.0
7	16.0	33.2	22.8	36.2	21.3	37.3	21.6	37.7
6/4	3.04	2.26	3.29	2.56	3.46	2.40	3.71	2.90

EIGENVECTORS Table 2.

PC	DATE	FOREST	DENSE URBAN	AIRPORT	DOWNTOWN	WHOLE IMAGE
1	Nov 82	-48.11	-35.94	-21.64	65.1	85.52
	March 84	+42.25	51.85	74.03	132.24	126.77
	Nov 82 + March 84	-50..03	-28.41	+24.75	+142.56	152.84
2	Nov 82	130.50	137.02	150.79	102.78	50.04
	March 84	169.29	168.82	172.94	77.01	89.79
	Nov. 82 + March 84	+200.95	206.11	212.01	110.84	108.06
3	Nov 82	23.78	-0.34	10.85	66.94	26.25
	March 84	-18.24	-4.80	-22.75	44.67	13.99
	Nov 82 + March 84	55.22	74.21	57.40	81.31	23.40

FIG 1.

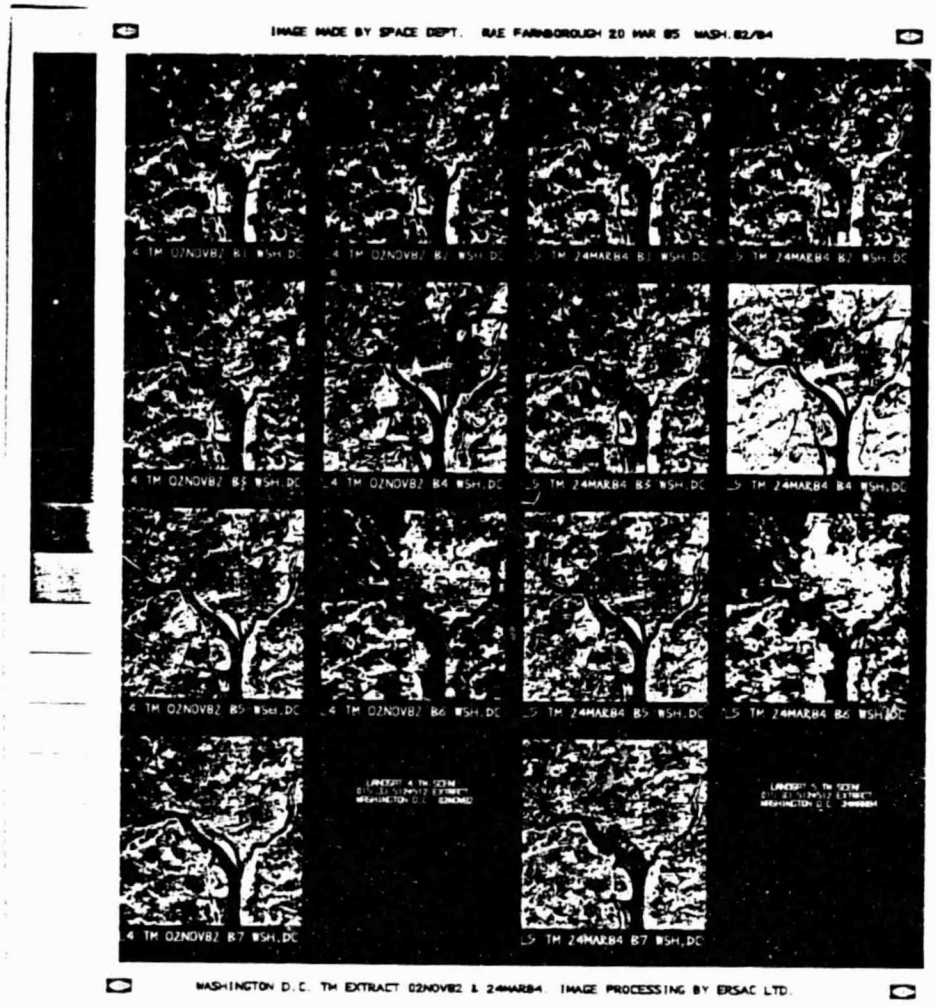

FIG 3

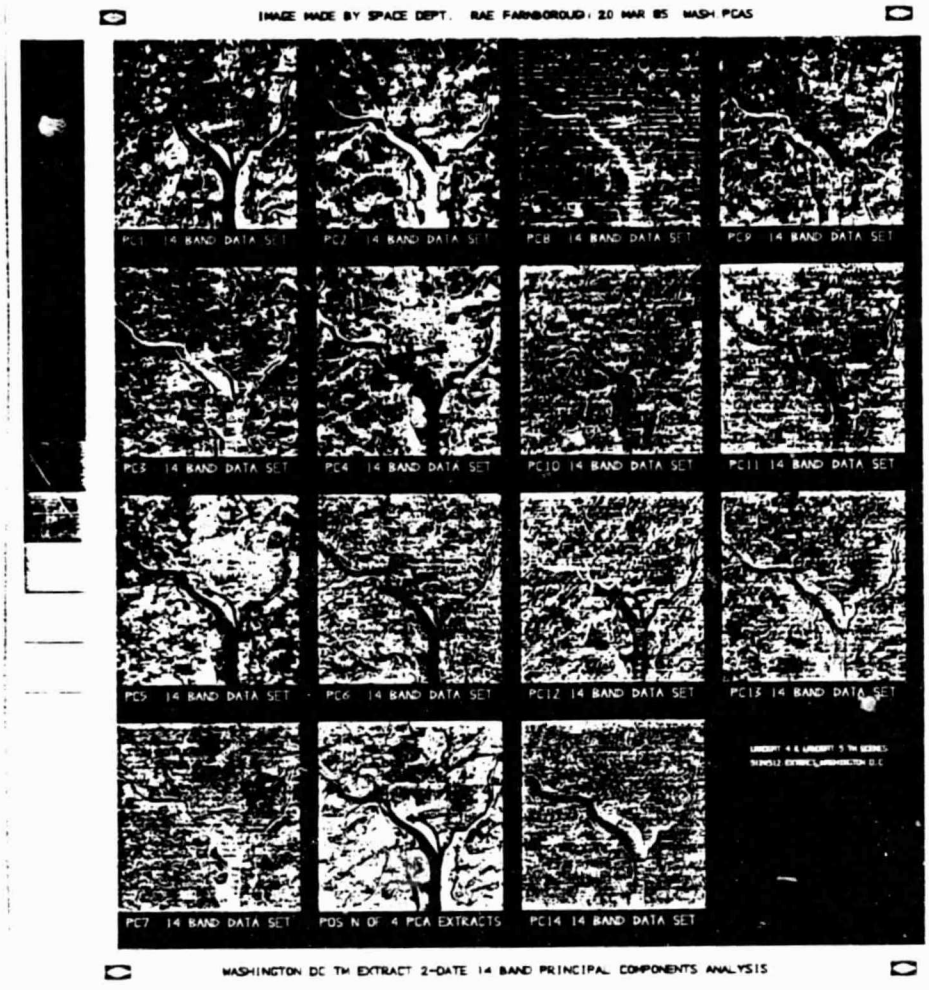

FIG 5

ORIGINAL PAGE IS
OF POOR QUALITY

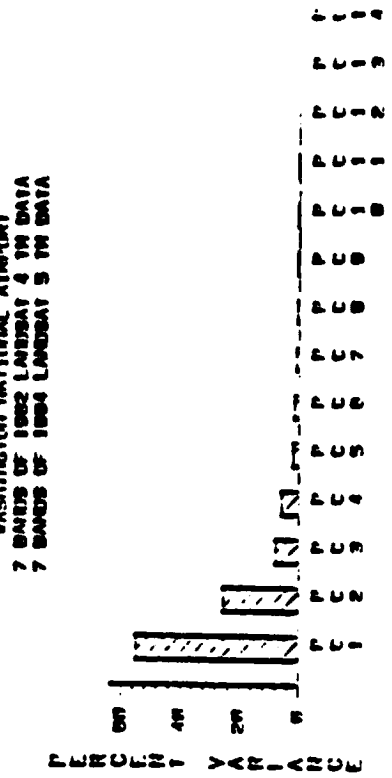

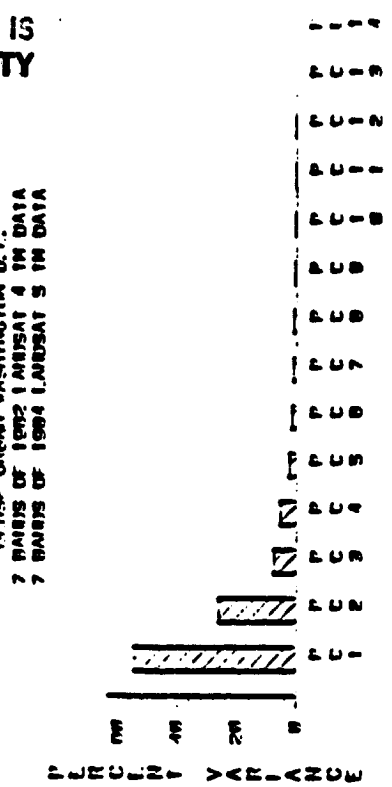

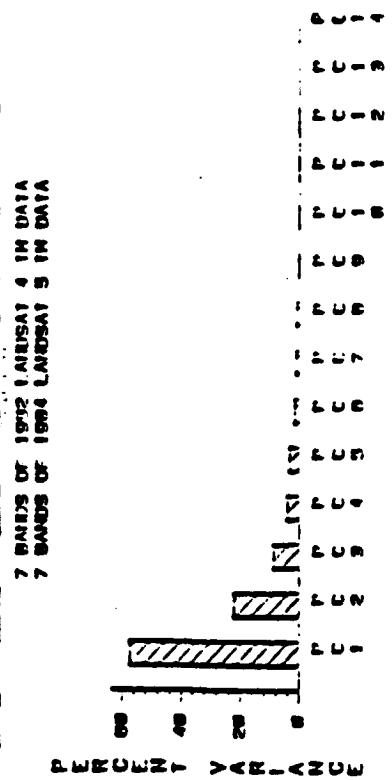

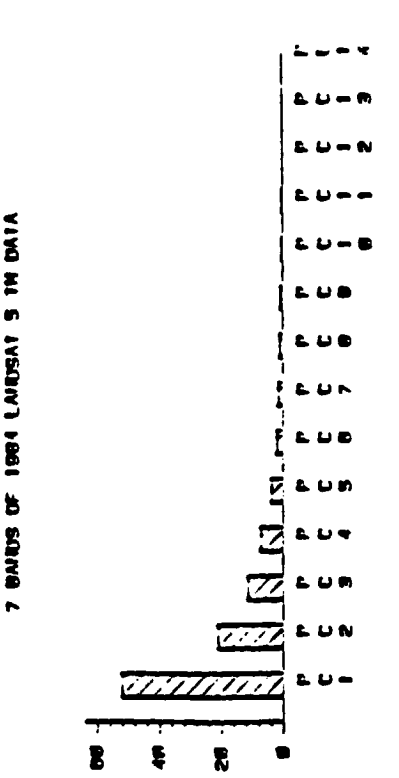

PRECEDING PAGE BLANK NOT FILMED

FIG 6

FOREST
7 BANDS OF 1982 LANDSAT 4 TM DATA
7 BANDS OF 1984 LANDSAT 5 TM DATA

FIRST PRINCIPAL COMPONENT

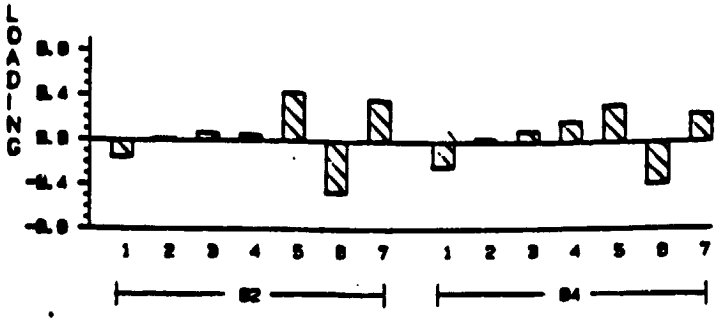

FEATURE VECTOR
(RADIANCE IN TM BANDPASSES)

FOREST
7 BANDS OF 1982 LANDSAT 4 TM DATA
7 BANDS OF 1984 LANDSAT 5 TM DATA

SECOND PRINCIPAL COMPONENT

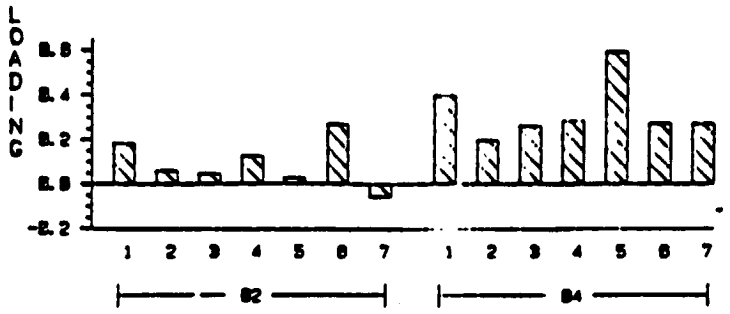

FEATURE VECTOR
(RADIANCE IN TM BANDPASSES)

FOREST
7 BANDS OF 1982 LANDSAT 4 TM DATA
7 BANDS OF 1984 LANDSAT 5 TM DATA

THIRD PRINCIPAL COMPONENT

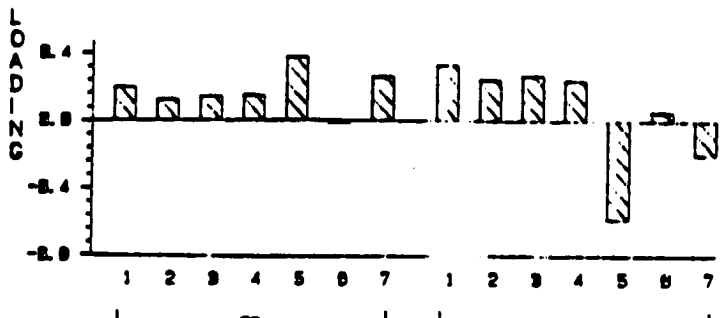

FEATURE VECTOR
(RADIANCE IN TM BANDPASSES)

WASHINGTON NATIONAL AIRPORT
7 BANDS OF 1982 LANDSAT 4 TM DATA
7 BANDS OF 1984 LANDSAT 5 TM DATA

FIRST PRINCIPAL COMPONENT

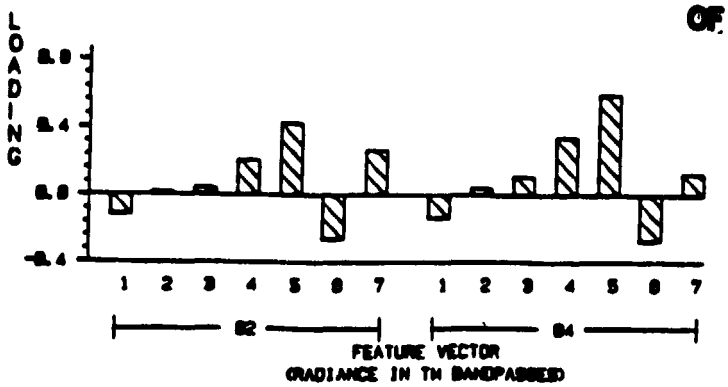

WASHINGTON NATIONAL AIRPORT
7 BANDS OF 1982 LANDSAT 4 TM DATA
7 BANDS OF 1984 LANDSAT 5 TM DATA

SECOND PRINCIPAL COMPONENT

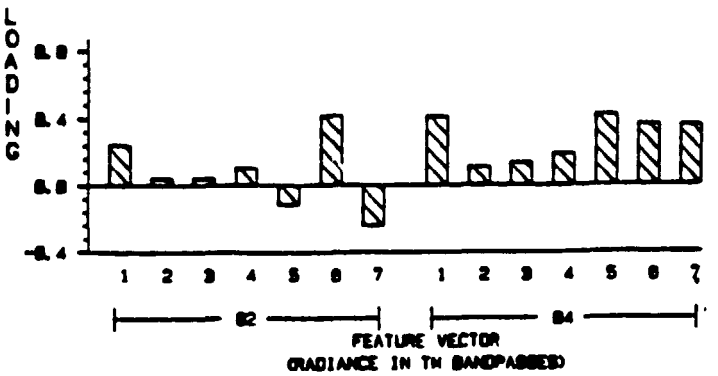

WASHINGTON NATIONAL AIRPORT
7 BANDS OF 1982 LANDSAT 4 TM DATA
7 BANDS OF 1984 LANDSAT 5 TM DATA

THIRD PRINCIPAL COMPONENT

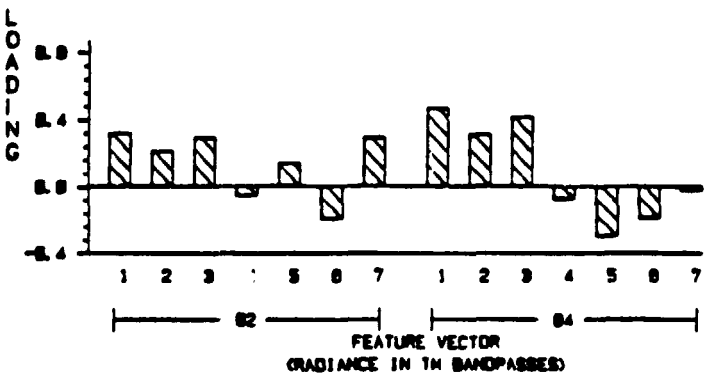

DENSE URBAN WASHINGTON D.C.
7 BANDS OF 1982 LANDSAT 4 TM DATA
7 BANDS OF 1984 LANDSAT 5 TM DATA

FIRST PRINCIPAL COMPONENT

FEATURE VECTOR
(RADIANCE IN TM BANDPASSES)

DENSE URBAN WASHINGTON D.C.
7 BANDS OF 1982 LANDSAT 4 TM DATA
7 BANDS OF 1984 LANDSAT 5 TM DATA

SECOND PRINCIPAL COMPONENT

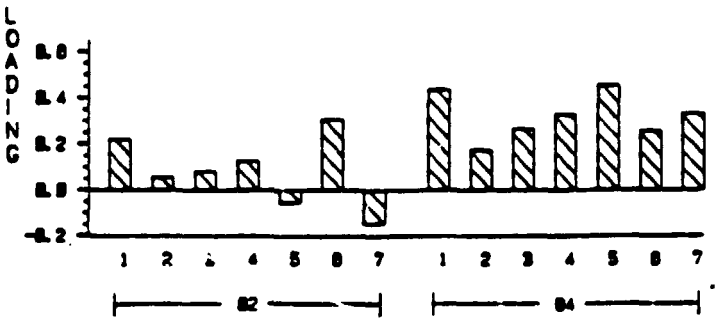

FEATURE VECTOR
(RADIANCE IN TM BANDPASSES)

DENSE URBAN WASHINGTON D.C.
7 BANDS OF 1982 LANDSAT 4 TM DATA
7 BANDS OF 1984 LANDSAT 5 TM DATA

THIRD PRINCIPAL COMPONENT

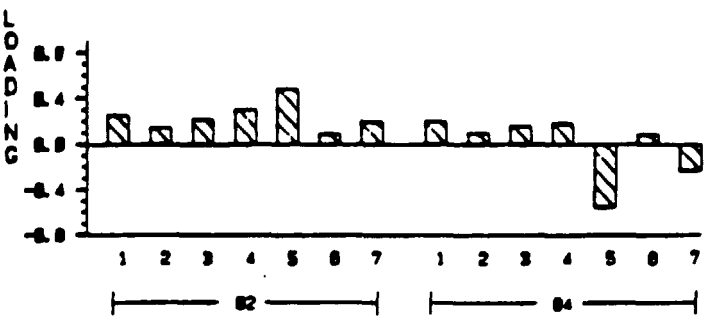

FEATURE VECTOR
(RADIANCE IN TM BANDPASSES)

DOWNTOWN WASHINGTON D.C.
7 BANDS OF 1982 LANDSAT 4 TM DATA
7 BANDS OF 1984 LANDSAT 5 TM DATA

FIRST PRINCIPAL COMPONENT

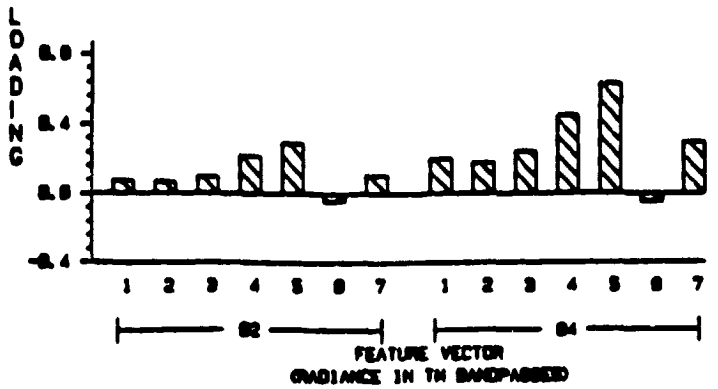

DOWNTOWN WASHINGTON D.C.
7 BANDS OF 1982 LANDSAT 4 TM DATA
7 BANDS OF 1984 LANDSAT 5 TM DATA

SECOND PRINCIPAL COMPONENT

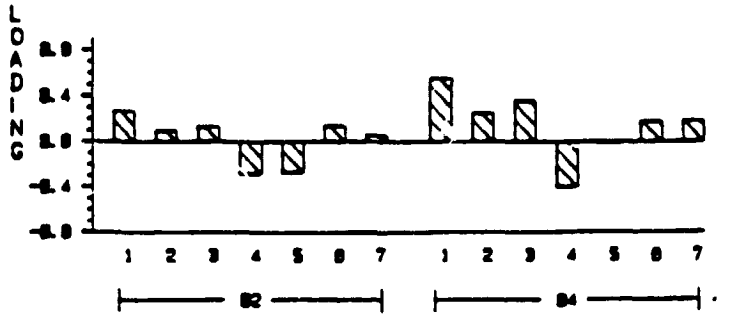

DOWNTOWN WASHINGTON D.C.
7 BANDS OF 1982 LANDSAT 4 TM DATA
7 BANDS OF 1984 LANDSAT 5 TM DATA

THIRD PRINCIPAL COMPONENT